The Gut Microbiome Modulates the Functionality of CD71+ Erythroid Cells in the Newborn

by

Yasaman Bahojb Habibyan

A thesis submitted in partial fulfillment of the requirements for the degree of

Master of Science

Medical Sciences – Oral Biology

University of Alberta

Abstract

Mounting preclinical and clinical evidence strongly supports the crucial role of the gut microbiota in health. A dysbiosis of the microbiome, an imbalance of the microbial populations, may predispose newborns to develop various immune disorders later in life, such as Inflammatory Bowel Disease (IBD) and Type 1 Diabetes (T1D). Thus, it is fundamental to investigate the mechanism by which the immune system can tolerate and coexist with the microbiome. It has been shown that CD71+ erythroid cells (CECs) are abundant in newborns relative to adults. The removal of CECs from the intestinal tissues by the anti-CD71 antibody disrupts immune homeostasis and results in inflammation. This suggests an essential role for CECs in the adaptation of newborns to colonization with microbial communities. Therefore, I sought to characterize $CD45^-$ and $CD45^+$ CECs in the gut and spleen of newborn mice. I looked at the expression of V-domain immunoglobulin suppressor of T cell activation (VISTA), transforming growth factor-beta (TGF-β), reactive oxygen species (ROS), and arginase-1. I found that $CD45^+$ CECs in newborns had higher expression of all measured immune factors relative to $CD45^-$ CECs in both the gut and the spleen. I next sought to characterize $CD45^-$ and $CD45^+$ CECs in SPF and GF mice. I found that $CD45^-$ and $CD45^+$ CECs from germ-free (GF) mice significantly lower the expression of immune mediators relative to specific-pathogen-free (SPF) mice. I next assessed the expression of toll-like receptors (TLRs) by CECs in SPF mice. I found that $CD45^+$ CECs had significantly higher expression of TLRs relative to $CD45^-$ CECs. These findings indicate that CECs, specifically the $CD45^+$ CECs are capable of microbial sensing and differ phenotypically in the absence of the microbiome. Finally, I explored whether a single depletion of CD71 on day 3 was sufficient to cause long-term microbial dysbiosis by either day

22 or day 36. I found that a single early depletion of CD71 did not result in long-term microbial dysbiosis by day 22. However, interestingly, by day 36 I found significant differences in beta diversity. These preliminary findings indicate that there is an interaction between CECs and the microbiome in early life. These results may be combined with ongoing research to potentially identify a novel and critical role for CECs in immune tolerance and microbial dysbiosis.

Preface

All experiments were done in the Elahi lab supported under CIHR grants. The thesis is being defended under the supervision of Dr. Febbraio. Therefore, Dr. Elahi was unable to verify the data presented in this thesis.

Table of Contents

List of Tables

List of Figures

1. Introduction

1.1 The Microbiome

1.1.1 Role of the Microbiome in Health

The microbiota within the gastrointestinal (GI) tract is composed of approximately 40 trillion microorganisms (1). These microorganisms play a crucial role in human health through their involvement in various processes such as metabolism, digestion, immune regulation, nervous system function, and protection against pathogens (2). It has been shown that changes to the intestinal microbiome from antibiotic usage resulted in altered neuronal signalling in the GI tract (3). Similarly, De Vadder and colleagues demonstrated that the enteric nervous system (ENS) of germ-free (GF) mice was immature relative to mice housed under conventional conditions. GF mice lack a microbiome: essentially, they are completely sterile (4). It was exhibited that colonization of GF mice with a healthy microbiome resulted in normalized ENS function (5). Moreover, the bacteria in the GI tract metabolize undigested carbohydrates. Products of these metabolic processes include short-chain fatty acids (SCFAs) (6). SCFAs are beneficial for many reasons, one of which is the maintenance of the mucosal layer and the epithelium (7). Moreover, SCFAs function as inhibitors of histone deacetylases (HDACs): this process promotes an anti-inflammatory immune system which promotes tolerance (8). Furthermore, the gut microbiota functions as a physical barrier against pathogenic microorganisms. The resistance provided against pathogens by the gut microbiome is referred to as colonization resistance (9). The residential bacteria obstruct the colonization of pathogenic bacteria through various mechanisms, such as nutrient competition (10).

Additionally, certain bacteria, such as *Bifidobacterium,* produce antimicrobial peptides (AMPs) (11). AMPs are also produced by the innate immune system to kill pathogenic microorganisms (12). Thus, the proper establishment of the microbiome is essential to human health.

1.1.2 Establishment of the Early Microbiome

The first few hours, days and weeks of an infant's life are critical for the establishment of the microbiome. Many different factors influence the composition of a newborn's microbiome, the first of which is whether the child is delivered via cesarean section (CS) or vaginal birth (Figure 1) (13). During vaginal delivery, the infant experiences microbial inoculation via the vaginal flora in the birth canal. This is fundamental since these microbes deoxygenate the gut (14). This allows for the establishment of strictly anaerobic bacteria, such as *Bacteroides* or *Bifidobacterium*, both important genera of bacteria in the newborn gut (15). Alternatively, infants delivered via CS do not experience the vaginal microbiome during birth. The lack of vaginal flora may explain why CS is associated with several long-term health challenges (16) (17).

During the first few months of the infant's life, their microbiome depends highly on the mother, since they primarily feed on the mother's breastmilk. Accordingly, *Bifidobacteriaceae* is present at high levels, since this family of bacteria can metabolize human milk oligosaccharides. *Bifidobacteriaceae* are involved in various events which are favourable for the infant. They are associated with a reduced risk of developing allergies and an improved immune response to vaccination (18) (19). It is important to note the difference in microbial compositions of

breastfed versus formula-fed infants (20). Ma and colleagues found that infants who were exclusively breastfed experienced lower microbial diversity compared to formula-fed infants. This is due to the composition of the mother's breastmilk; oligosaccharides are a metabolic source for only a limited number of bacterial strains (21). Following the introduction of solid food, there is a substantial expansion of the microbiome with an increase in diversity (Figure 1). Moreover, sex is another critical driver of microbial composition that can influence the microbiome as early as from birth. Research has shown that sex hormones, such as estrogen and testosterone, interact with and influence the composition of the microbiome (22,23). In fact, several studies have shown these sex-related differences in both mouse and human models (22–25). However, since early childhood is characterized by gonadal hormone quiescence sex-specific differences in the microbiome only begin to emerge during puberty (26–28). Yurkovetskiy and colleagues examined the role of sex on the microbiome during pubescence, adolescence, and adulthood in mice. They found that the male microbiome diverged during adulthood while the female adult microbiome resembled that of the pubescent period (29). Essentially, the proper establishment of a microbiome during this period is crucial for lifelong health. Various studies have implicated the importance of proper microbiome development in the development of immune disorders and allergies (30).

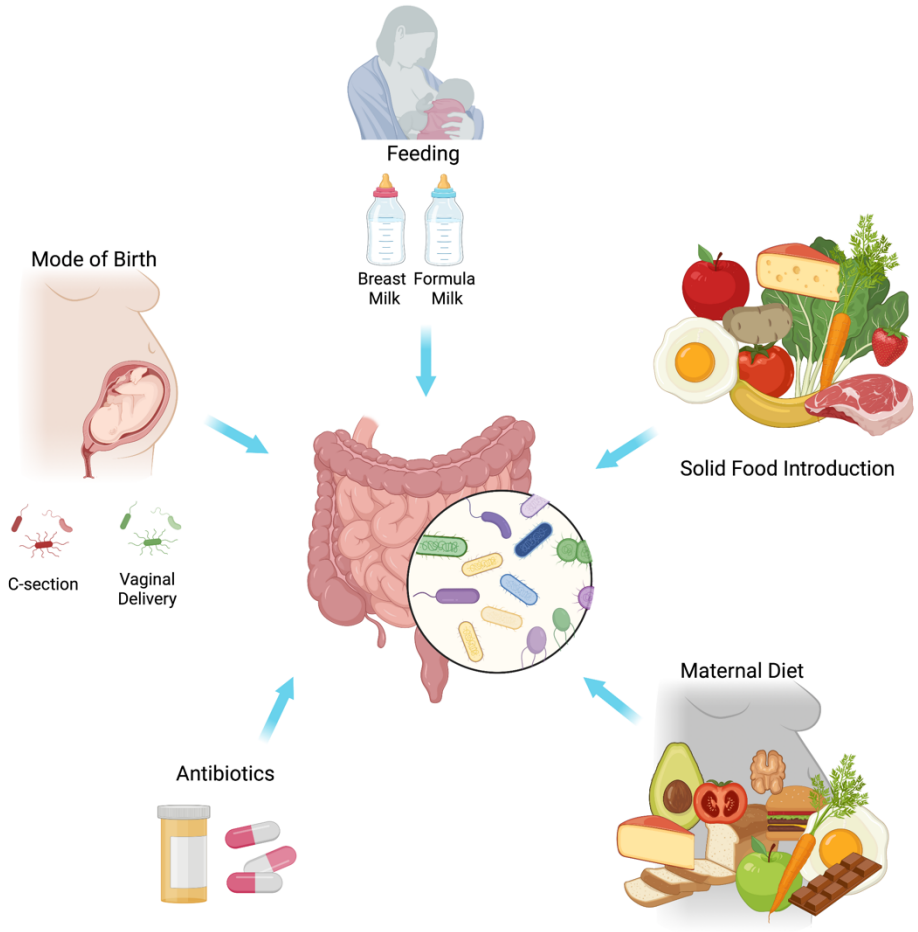

Figure 1: Factors Impacting the Gut Microbiome of Newborns.

During pregnancy, the fetus is supported through the mother's diet and metabolites produced from the microbiome. During birth, the newborn is first exposed to foreign bacteria. At this time the infant's immune response is still largely dependent on immune factors found in the mother's milk. During the early stages of the newborn's life, the major effectors of microbial composition and immune response are birth route, breast milk vs formula milk, and antibiotics. As the child shifts to a solid food diet, there is a large shift in microbial composition with an increase in diversity. This time in a child's life is often referred to as the "window of opportunity" because proper development at this stage is crucial for life-long health, the evolving microbiota, and the mucosal immune system. IBD, inflammatory bowel disease; T1D, type 1 diabetes. Figure adapted from Cresci and Izzo 2019 (31)

1.2 How the Immune System Detects and Tolerates the Microbiome

The immune system is constantly faced with a challenge pertaining to the microbiome. The immune system must establish and maintain tolerance to the indigenous and commensal bacterial strains present while being able to initiate an effective immune response against pathogenic strains. It is important to understand how the immune system can maintain a tolerant environment for the proper colonization of the microbiome.

The innate immune system utilizes pattern recognition receptors (PRRs) to detect microorganisms (32) (33). PRRs are composed of both membrane-bound and cytosolic receptors. Toll-like receptors (TLRs) are membrane-bound and can be found on the cell surface as well as intracellularly (34). Alternatively, nucleotide-binding oligomerization domain-like receptors (NOD-like receptors, NLR) and retinoic acid-inducible gene-I-like receptors (RIG-like receptors, RLR) are both cytosolic receptors. These different classes of PRRs can sense highly conserved structures such as lipopolysaccharide (LPS) and peptidoglycan (35). These structures are referred to as pathogen-associated molecular patterns (PAMPs) (36). PAMPS are not produced by eukaryotic, or host cells (37). Hence, through PRR signalling, the innate immune system can differentiate molecular structures of microbial invaders from self. Since the targets of PRRs are very highly conserved structures among microbes they are not able to differentiate between pathogenic and commensal strains. The exact mechanism by which the host immune system can tolerate commensal microbes is not known. However, it is thought to be due to a combination of anti-inflammatory cytokines as well as the confinement of bacteria to the lumen side of the Gi tract (38).

1.3 Structure of the GI Tract

The entirety of the GI tract is covered in a layer of mucus which is produced by goblet cells and serves as the first line of defence for the innate immune system (39). The mucus provides a physical barrier that protects the intestinal epithelial cell layer. This is essential to protect against unwanted activation of the immune system through interactions with antigens, toxins, pathogens, and microbiota (40).

The next layer of defence underneath is the intestinal epithelium. The intestinal epithelium is composed of a single layer of intestinal epithelial cells (IECs) that are organized into crypts and villi. IECs are comprised of enterocytes, endocrine cells, microfold cells (M cells), goblet cells, and Paneth cells (41). The collective of these cells together forms a defence against the contents of the lumen while maintaining selective permeability to allow for the absorbance of nutrients and water. This selective barrier function is made possible by a network of proteins such as tight junctions. It is essential to maintain a tight barrier between the lamina propria and the antigens, toxins, pathogens, and microbiota that can be found in the lumen (41). The lamina propria is a loose connective tissue layer found directly beneath the epithelium (42). The epithelial barrier protects from any unwanted immune reaction that may result; alterations in the barrier are thought to play a role in the pathogenesis of GI diseases (41).

1.4 Microbial Dysbiosis and Immune Function

A balanced microbiome is needed for the proper development of the GI tract and immune system. A dysbiosis of the microbiome, an imbalance of the microbial populations, may

predispose newborns to develop various immune disorders later in life, such as asthma, inflammatory bowel disease (IBD), and type 1 diabetes (T1D) (43) (44). The role of the microbiome in proper immune function is an area of research that has gained a great deal of interest over the years. It has been shown that individuals with IBD experience a reduction in bacterial diversity, specifically, it has been noted that there is a reduction in the anti-inflammatory strains of bacteria (45).

1.5 The Germ-Free Mouse Model

The role of the microbiome in proper immune development and function has been greatly studied using the GF mouse model (4). It has been shown that these mice experience dysfunctional immune development. Specifically, in the GI tract, there are deficiencies in the formation of Peyer's patches and the gut-associated lymphoid tissues (GALT) (46) (4). Furthermore, it has also been shown that GF mice express reduced levels of several TLRs (47,48). Interestingly, Hernández-Chirlaque and colleagues found that GF mice were more susceptible to dextran sulphate sodium (DSS)-induced colitis. They found that GF mice experienced increased blood loss and higher mortality rates, and became more physically ill, compared to mice housed under conventional conditions (49). DSS is commonly used as a model for IBD in mice to study the pathogenesis of the disease and possible therapies (50).

1.6 CD71+ Erythroid Cells

CD71+ erythroid cells (CECs) are a class of immature nucleated and unnucleated erythrocytes. CECS are identified as being CD71 (transferrin receptor) and TER119 (erythroid lineage marker)

positive in mice and CD71 and CD235a (erythroid lineage marker) positive in humans (Figure 2) (51). In healthy adults, CECs are virtually exclusive to the bone marrow. However, CEC frequency increases under physiological stress and pathological conditions (51). Unlike in adults, it has been shown that CECs are enriched in the neonatal spleen of both mice and humans (52) (53). The generation of erythrocytes outside the bone marrow is referred to as extramedullary erythropoiesis (EE) (54). During EE, a primary site of CEC generation is the spleen. The spleen is a secondary lymphoid organ and is responsible for filtering blood to ensure the removal of waste and dead cells. The spleen is also involved in generating leukocytes, erythrocytes, and platelets (55). Thus, EE produces elevated levels of CECs in the spleens of newborn mice in comparison to adults, this persists for the first 4 weeks of life in mice. Some other conditions that lead to EE and an increase in the frequency of CECs are anemia, pregnancy, and infection (56–58).

1.6.1 CD45 (lymphocyte receptor antigen)

A notable marker expressed by CECs is CD45. CD45 (lymphocyte receptor antigen) is a receptor-linked protein tyrosine phosphatase (PTP). It is also known as protein tyrosine phosphatase receptor type C (PTPCR). CD45 is one of the most abundant cell surface glycoproteins, encompassing up to ten percent of the cell surface area (59). There are many different isoforms of CD45 that may be generated; this is due to alternative splicing (60). The expression of CD45 isoforms is cell type-specific; it is also reliant on the stage of differentiation as well as the activation status of the cells (61). CD45 is expressed on all hematopoietic cells, excluding mature erythrocytes and platelets (60). $CD45^-$ CECs are more mature in comparison to the

$CD45^+$ population of CECs (Figure 2). CD45 involvement in immune function has been best characterized in T cells. It has been shown that CD45 expression is necessary for antigen-induced CD4+ T cell activation. Pingel and Thomas demonstrated that CD45 deficient CD4+ T cells were unable to proliferate in response to antigen, however, their basal proliferative response was maintained (62). Notably, it has been found that $CD45^+$ CECs from adult mice expressed higher levels of immune mediators relative to $CD45^-$ CECs (56).

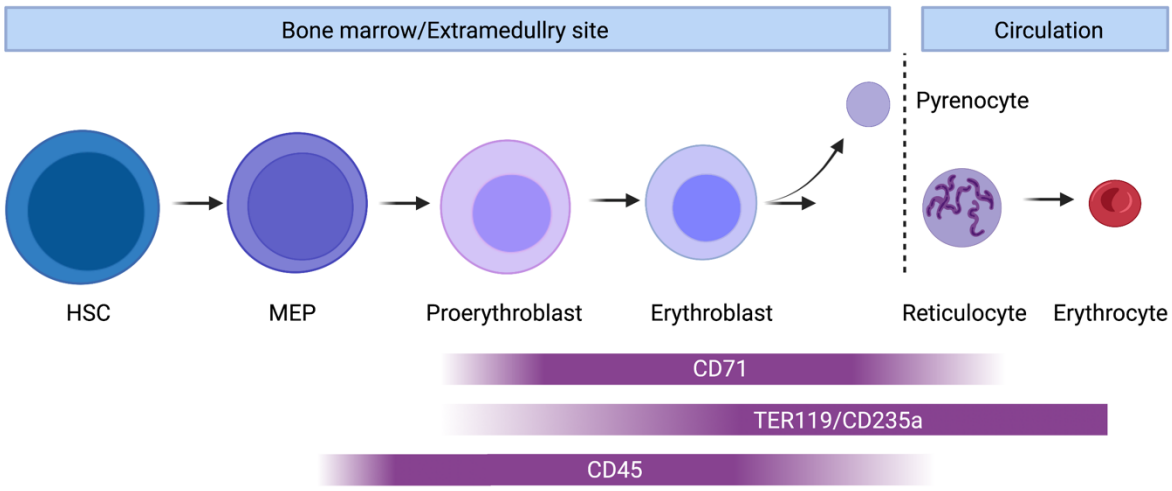

Figure 2: Development of Erythrocytes and Timeline of CD71+ Erythroid Cells.

A hematopoietic stem cell (HSC) develops into a megakaryocyte–erythroid progenitor cell (MEP). The proerythroblast then develops into an erythroblast. By the process of denucleation, the erythroblast loses its nucleus, releasing a pyrenocyte (a membrane-enclosed nucleus). The erythroblast now lacks a nucleus and is referred to as a reticulocyte and can be found in the circulation. Finally, the reticulocyte forms into a mature erythrocyte that is $CD71^{-}$ $TER119^{+}$. Figure adapted from Grzywa et al. 2021 (63).

1.6.2 CECs and Their Role in Pregnancy and Newborn Health

Interestingly, CECs are present in the cord blood and placenta tissues during pregnancy (57). During pregnancy, the immune system must be in a cooperative state to allow for the retention of the fetus. Previous data indicate that both the frequency and functionality of CECs are impaired in pregnant women with inflammatory bowel disease (IBD). There was not only a decrease in the frequency of CECs from the cord blood of pregnant women with IBD but also a dysfunction in the immune regulatory capabilities of the cells when plated *in vitro* with naïve T cells. Dunsmore and colleagues demonstrated that depletion of CECs from the cord blood mononuclear cells (CBMC) of healthy mothers resulted in an increase in proliferation of CD4+ and CD8+ T cells; this phenomenon was not observed in CBMCs of pregnant women with IBD (57). This points to an important role of CECs in the maintenance of a tolerative immune environment. Originally it was believed that the high susceptibility of infants to infections was due to an immature immune system. However, recent findings suggest that this susceptibility is rather due to active immune suppression. Dunsmore and colleagues showed that neonatal CECs had immune suppressive effects against *Bordetella pertussis*. Newborns were much more susceptible to *B. pertussis* infection in comparison to adults. Moreover, the adoptive transfer of neonatal CECs to adult mice resulted in impaired immune protection against infection (58). Previous studies have sought to establish which mechanisms are used by CECs to maintain immune suppression. Immune suppression by CECs may be in part due to the expression of V-domain immunoglobulin suppressor of T cell activation (VISTA), transforming growth factor-beta (TGF-β), reactive oxygen species, and arginase-1 which will be discussed in future sections.

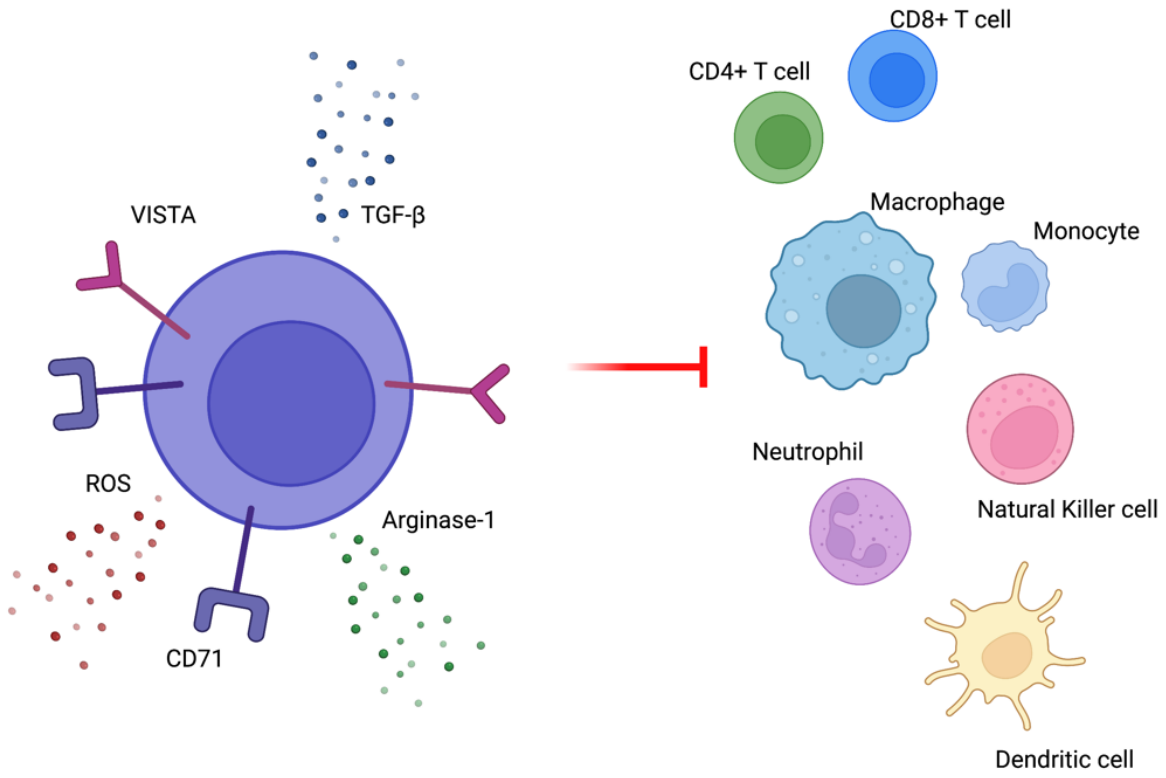

Figure 3: The functionality of CD71+ Erythroid Cells.

CD71+ erythroid cells (CECs) have been shown to have immune-suppressive properties through the expression of various receptors/ligands and soluble factors. VISTA = V-domain immunoglobulin suppressor of T cell activation. ROS = reactive oxygen species. TGF-β = Transforming growth factor-β.

1.6.3 V-domain Immunoglobulin Suppressor of T Cell Activation (VISTA)

VISTA is an immune regulatory receptor belonging to the B7 family (64). It is primarily expressed on hematopoietic cells, such as neutrophils, monocytes, macrophages, and dendritic cells (DCs) (65). VISTA possesses many structural homologies to other receptors in the B7 family such as CD28, CTLA-4 and PD-1, however, it does not contain an ITIM/ITAM motif (65,66). VISTA signals by binding to either V-set and Ig domain-containing 3 (VSIG3) and P-selectin glycoprotein ligand 1 (PSGL-1) ligands; bidirectional signalling may occur since VISTA can function as both a receptor and a ligand (67). Wang and colleagues showed that the absence of VISTA in mice resulted in immune alterations. Mice who genetically lacked VISTA accumulated T cells, which was accompanied by an increase in the production of inflammatory cytokines and chemokines. These findings indicate that loss of VISTA leads to a reduction in the threshold of T cell activation (68). Notably, Shahbaz and colleagues demonstrated that neonatal CECs expressed significant levels of VISTA. Moreover, they showed that the $VISTA^{+}$ subset of CECs expressed significantly higher levels of TGF-β in comparison to $VISTA^{-}$ CECs (69).

1.6.4 Transforming Growth Factor-Beta (TGF-β)

TGF-β is a well-known anti-inflammatory cytokine. TGF-β is known to play a role in immune regulation, wound healing, angiogenesis, and cancer. TGF-β promotes the differentiation of CD4+ naïve T cells into Foxp3+ regulatory T (Treg) cells while suppressing effector T cell activation and proliferation (70) (71). Treg cells are characterized into two categories: thymic Treg (tTreg) cells and peripherally induced Treg (pTreg) cells. tTregs constitutively express Foxp3 before leaving the thymus, therefore they are not reliant on TGF-β. However, pTregs

develop from naïve CD4+ T cells exposed to antigens under tolerogenic conditions, thus requiring TGF-β (72). Treg cells play a crucial role in the immune tolerance to self-antigens and thus control autoimmune reactions (73). Levéen and colleagues demonstrated that mice deficient in the TGF-βRII receptor experienced inflammatory infiltration in several organs and uncontrolled T cell proliferation (74). Moreover, T cells that expressed dominant-negative TGF-βRII receptor led to unchecked proliferation and inflammatory and autoimmune-like diseases (75) (76). These studies demonstrate TGF-β–dependent signals in T cell activation and tolerance *in vivo.*

1.6.5 Reactive Oxygen Species (ROS)

ROS are small, oxygen-containing, short-lived, highly reactive molecules. There are over 20 different subtypes of ROS (77). The effects of ROS on the immune response can be variable and promote both inflammatory responses as well as immune suppression. Notably, Srivastava and colleagues demonstrated that Myeloid-derived Suppressor Cells (MDSCs) inhibited CD4+ and CD8+ T cell activation through the depletion of cystine and cysteine; this process is heavily reliant on ROS (78). Moreover, Olofsson and colleagues demonstrated the importance of ROS in immune regulation using rats with mutated alleles of the neutrophil cytosolic factor 1 (Ncf1) gene, that encoded a less functional nicotinamide adenine dinucleotide phosphate (NADPH) oxidase 2 (Nox2). Nox2 is involved in the generation of ROS (79). In this study, Olofsson and colleagues showed that the rats with the mutated Ncf1 alleles were more prone to autoimmune inflammation compared to their littermates (80). This indicates the role of ROS in the prevention of autoimmune activation.

1.6.6 Arginase-1

Previous findings showed that arginase activity is essential for the immune suppressive abilities of CECs (53). Arginase-1 catalyzes the breakdown of arginase to urea. Arginase-1 is also involved in the immune response. El Kasmi and colleagues established that the induction of arginase-1 through TLR signalling in macrophages resulted in a blunting of the immune response after *Mycobacterium tuberculosis* infection. They also exhibited that the increase in arginase-1 limited the production of nitric oxide (NO) by macrophages. This is significant since NO production by macrophages plays an antimicrobial role. Moreover, they showed that the elimination of arginase-1 from macrophages resulted in favoured host survival and decreased bacterial load in the lungs during tuberculosis infection (81). Another study conducted by Pesce and colleagues presented that arginase-1 is essential for alternatively activated macrophage (AAM) immune suppression. They showed that macrophages which expressed arginase-1 suppressed Th2-dependent inflammation and fibrosis (82).

1.7 Gap of Knowledge

The proper establishment of the microbiome is essential for overall health. Specifically, the first few days, weeks, and months of an infant's life are critical for the establishment of the microbiome. Hence, it is vital that the immune system can appropriately tolerate the colonization of the microbiome. CECs have been shown to be enriched in newborns relative to adults. It has also been shown that CECs possess immunosuppressive properties. Furthermore, it has been shown that when CD71 is depleted, the immune homeostasis in the gut is disrupted. Previous data showed that this depletion resulted in higher levels of inflammatory cytokines in

the environment. This indicates that the presence of CECs may inhibit unwanted immune activation and aid in the induction of tolerance. It is feasible that they promote the induction of immune tolerance towards the colonization of the microbiome. However, studies have yet to be conducted exploring the relationship between CECs and the establishment of a healthy microbiome. The overriding questions that I will address in my thesis are whether the microbiome has any impact on the functionality of both $CD45^-$ and $CD45^+$ CECs and whether CECs are required for the proper establishment of the microbiome in newborns.

1.8 Aims, Hypothesis, Significance

Aim 1A To characterize the CEC populations in the spleen and gut of newborns using flow cytometry. The functionality of $CD45^-$ and $CD45^+$ CECs was assessed by the expression of VISTA, TGF-β, ROS, and arginase-1.

Hypotheses 1A I hypothesize that $CD45^+$ CECs in newborns will be more potent immune mediators due to the higher expression of VISTA, TGF-β, ROS, and arginase-1 relative to $CD45^-$ CECs. I also hypothesize that the $CD45^-$ and $CD45^+$ CECs in the gut will have greater expression of VISTA, TGF-β, ROS, and arginase-1 relative to $CD45^-$ and $CD45^+$ CECs in the spleen.

Aim 1B To investigate the role of the microbiome in CEC functionality through the expression of VISTA, TGF-β, ROS, and arginase-1 in the spleen and gut of specific pathogen-free (SPF) mice relative to GF mice.

Hypothesis 1B I hypothesize that $CD45^-$ and $CD45^+$ CECs from GF mice will have lower expression VISTA, TGF-β, ROS, and arginase-1 when compared to SPF mice due to the absence of a commensal microbiome.

Aim 1C To investigate whether $CD45^-$ and $CD45^+$ CECs can sense microorganisms through TLR expression.

Hypothesis 1C I hypothesize that $CD45^-$ and $CD45^+$ CECs express TLRs.

Aim 2 To investigate whether a single depletion of CECs in newborns has long-lasting effects on microbial composition during weaning and post-weaning periods. This was done through the depletion of CD71 on day 3 using an anti-CD71 antibody. The first litter was left until the weaning period, or day 22, and the second litter was left until two weeks post-weaning period, or day 36. Microbial analysis was then done from the small intestine.

Hypothesis 2 I hypothesize that CECs allow for the colonization of a commensal microbiome in the GI tract of newborns upon exposure to the external world, and their depletion on day 3 will result in microbial dysbiosis on days 22 and 36.

The characteristics of $CD45^-$ and $CD45^+$ CECs in the gut and spleen of newborns have never been investigated. My findings will provide new data concerning the phenotypes of these cell populations in different tissues. Moreover, my comparisons of CECs in SPF and GF mice may unlock an innovative role for CECs in the immune tolerance of microbial colonization in infants through microbial sensing by CECs. Furthermore, my second aim will answer whether a single depletion of CECs at an early age is sufficient to predispose mice to long-term microbial dysbiosis. My findings will contribute novel information that may help explain the dysbiosis of the microbiome that is observed in some newborns.

2. Materials and Methods

2.1 Mice

C57BL/6 (B6) mice were housed under SPF and GF conditions for experiments in aim 1. B6 mice were purchased from the Charles River Laboratory. The GF mice were raised in Axenic Mouse Research Unit at the University of Alberta; the GF mice were housed in tightly regulated and monitored isolators, and they were checked regularly to confirm GF status. Pups from each group were sacrificed at the time points: day 1, day 3, and day 6. The pregnancies were not matched between the SPF and GF litters, therefore the litters from corresponding time points were processed individually.

SPF-housed BALB/c mice were used for the microbiome experiments in aim 2. BALB/c mice were purchased from the Charles River Laboratory. All mice were maintained and bred within the animal care facility at the University of Alberta.

2.2 Ethics Statement

All experiments were performed in accordance with the Canadian Council on Animal Care guidelines and followed procedures approved by the University of Alberta Animal Policy and Welfare Committee (Protocol #AUP00001021).

2.3 CD71 Long-term Depletions

Litters of 10+ pups were used, and each litter of pups was randomly split into treated and control groups; treated mice received anti-CD71 antibody (150 µg, clone# 8D3, cat# 50-206-

5580) while control groups received rat IgG2a isotype control antibody (150 µg, cat# BE0089). Pups were all injected on day 3. There were two long-term time points selected: at weaning (day 22) and two weeks post-weaning (day 36).

2.4 Gut Cell Isolation

The small intestine and colon were removed and placed in complete media (RPMI 1640 Medium (with L-glutamine and sodium bicarbonate, liquid, sterile-filtered, Cat# R8758) + 10% Fetal Bovine Serum (FBS, Sigma, Cat# F1051-100ML) + 1% Penicillin/Streptomycin (Sigma, Cat#P0781-100ML) on ice. Tissues were then cleaned of connective tissue, stool, and mucus in cold complete media. Tissues were placed in an extraction buffer (30 mL RPMI, 93 µL 0.3M Dithiothreitol (DTT), 60 µL 0.3M Ethylenediaminetetraacetic acid (EDTA, Sigma, Cat# E5134), 500 µL FBS (Cat# F1051-100ML) and incubated in a shaker for 20 minutes at 37°C. After incubation, tissues were rinsed in cold Dulbecco's Phosphate Buffered Saline (PBS, Cat# D8537-100ML), to remove any remaining EDTA, before being transferred into the digestion buffer (25 mL RPMI, 300 µL collagenase type II (Cat# 17101015), 300 µL dispase (Cat# 07913), 300 µL FBS (Cat# F1051-100ML). Tissues were cut with scissors until the samples were homogenized. The samples were then incubated in a shaker for 30 minutes at 37°C. Next, the samples were filtered through 40 µm filters (Fisherbrand™ Sterile Cell Strainer, Cat# 352360) and an equal volume of complete media was added to stop any further digestion of samples. Finally, the samples were centrifuged for 10 minutes at 420 G-Force. The supernatant was discarded, and the pellet was resuspended in 200 µL of complete media.

,

2.5 Spleen Cell Isolation

The spleen was removed and placed on ice. The tissue was manually ground in 7 mL of RBC lysis buffer (8.3 gm/l NH4Cl in 0.01 M Tris–HCl buffer of pH 7.5) using frosted microscope slides. The mixture was left for 1-2 minutes in RBC lysis buffer to allow complete lysis of red blood cells. 7 mL of complete media were added to the mixture to neutralize the reaction. Samples were then centrifuged for 10 minutes at 360 G-Force. The supernatant was discarded, and the pellet was resuspended in 200 µL.

2.6 Preparation of Cells for Flow Cytometry

Cells were counted and 1,000,000 cells were placed from each sample into a U bottom 96-well plate for incubation with antibodies. Cells were then centrifuged for 3 minutes at 550 G-Force. The supernatant was discarded and cell pellets from each sample were then washed with cold, sterile Dulbecco's Phosphate Buffered Saline (DPBS, RNBJ5141). Cells were then centrifuged for 3 minutes at 550 G-Force and the supernatant was discarded. The supernatant was discarded, and cells were incubated with antibodies diluted in fluorescence-activated cell sorting (FACS) buffer (PBS with 2% FBS) (Table 1). For intracellular antigens (TGF-β, Arginase-1, and TLR9), cells were permeabilized using 200 µL of Fixation/Permeabilization Solution from the BD Cytofix/Cytoperm™ Fixation/Permeabilization Solution Kit (BD, Cat#BDB554714). The intracellular antibodies were then diluted in BD Perm/Wash™ Buffer (BD, Cat#BDB554714). The samples were then rinsed with BD Perm/Wash™ Buffer and fixed in a 4% paraformaldehyde (PFA) solution (PBS with 4% PFA).

2.6 Measuring Reactive Oxygen Species

2',7'-dichlorofluorescein diacetate ($DCFH_2$-DA, Sigma) was used to detect the intracellular generation of reactive oxygen species (ROS). The cells were then incubated with 100 uL of DCFDA (1/1000 dilution in sterile PBS). Samples were incubated in a 37°C CO_2 incubator for 30 minutes. 150 uL of cold PBS were then added to each sample before centrifuging for 3 minutes at 550 G-Force. Cells were then incubated with antibodies for flow cytometry followed as above. DCF fluorescence was measured by flow cytometry.

2.7 Flow Cytometry

Samples were acquired using a BD LSRFortessa^{TM} Cell Analyzer (BD Biosciences). The threshold was set to 20,000 cells for each experiment. For forward and side scatter, the area, height, and width were recorded. The voltages for all fluorophores were adjusted so that the positive peak lay between 10^3 and 10^5 on the log scale. A minimum of 100,000 cells were acquired for each sample. Compensation controls were recorded for each fluorophore.

2.8 Flow Cytometry Analysis

Flow cytometry standard (FCS) files obtained from each experiment were analyzed using FlowJo™ v10.8 Software (BD Life Sciences). First, the compensation controls were applied to each sample. A positive gate was set around live cells by plotting the Live/Dead stain (V525) and forward scatter (FSC). Then lymphocytes were selected by gating FSC and the side scatter (SSC). Next, single cells were selected by gating the FSC-A and FSC-H. Then CECs were gated by selecting TER119+CD71+ cells; these cells were then split into CD45- and CD45+. VISTA, ROS,

TGF-β, and arginase-1 were measured by geometric mean analysis of both CD45- and CD45+ CEC groups. VISTA was also measured with gating: a VISTA fluorescence minus one (FMO) was used to set the positive gate. TLR1 and TLR4 expressions were measured by both gating on positive populations as well as measuring the geometric mean. An FMO for each TLR was used to determine the positive gating. TLR9 expression was measured by geometric mean analysis.

2.9 Collection of Stool for Microbial Sequencing

50 mg of stool were isolated from the small intestine of each mouse and placed into a 2 mL screw top tube containing 5 metal beads each. The samples were incubated in a 95°C water bath for 10 minutes to ensure the lysis of Gram-positive bacteria. Bacterial DNA was isolated with the use of the QIAamp DNA Fast Stool Mini Kit (51604). Additionally, all samples were cleaned using the DNeasy PowerClean Pro Cleanup Kit (12997-50) to ensure all samples were of good quality before submission. Samples were submitted to the High Content Analysis Core at the University of Alberta. 16S rRNA sequencing was performed on the Illumina MiSeq by Sudip Subedi, High Content Analysis Core Technologist. The Nextera XT v2 Index Kit was used and the V4 variable region of the 16S rRNA gene was amplified.

2.10 Microbiome Analysis

Bioinformatic analysis was done using the QIIME2 pipeline (83). The first step was to import the demultiplex paired-end raw sequences into the QIIME2 environment. The samples were then quality filtered to trim the sequences to confirm all reads had a minimum Phred quality score of 20. The reads were de-noised using the Deblur method, and a feature table was created for the

samples. Alpha rarefaction was checked to ensure that all samples had sufficient sequencing depth to capture sample diversity. The next step in the analysis was to create a reference phylogenetic tree for phylogenetic diversity measures. The steps to achieve this were: multiple sequence alignment using MAFFT, masking the uninformative positions, building the phylogenetic tree using FastTree, and finally rooting the tree at the midpoint. The Green genes bacterial reference database (v. 13.8) was used to create a reference taxonomy which was compared to samples. Finally, the diversity core-metrics-phylogenetic QIIME2 command was used to analyze both phylogenetic and non-phylogenetic diversity measures.

2.11 Statistical Analysis

Statistical analyses were performed using Graph Pad Prism v.9.0. (GraphPad Software, San Diego, CA, USA). Results from flow cytometry analyses were analyzed using one-way ANOVA followed by Tukey's multiple comparisons. Results from the alpha diversity metrics in the microbial analysis were analyzed using the non-parametric double-check Kruskal-Wallis test. Results from the beta diversity unweighted and weighted UniFrac PCoA were analyzed using PERMANOVA. Finally, the taxonomic classifications were analyzed using non-parametric t-tests. A p-value less than 0.05 was considered significant. Only significant p-values are shown in the figures.

Table 1: List of Antibodies and Reagents used for Flow Cytometry

Antibodies	Clone	Fluorophore	Catalogue Number	Vendor
Live/Dead fixable Aqua	N/A	V525	L34966	Life Technologies
Monoclonal anti-mouse CD71	R17217	e450	48-0711-82	eBioscience
Monoclonal anti-mouse TER119	TER-119	Pe-Cy5	15-5921-83	Thermo Fisher Scientific
Monoclonal anti-mouse TER119	TER-119	FITC	557915	BD Bioscience
Monoclonal anti-mouse CD45	30-F11	Pe-Cy7	25-0451-82	Invitrogen
Monoclonal anti-mouse VISTA	MIH63	PE	150203	BD Bioscience
Monoclonal anti-mouse Arginase-1	IC5868A	APC	IC5868A	R&D
Monoclonal anti-mouse TGF-β	TW7-16B4	PE	563143	BD Bioscience
Monoclonal anti-mouse CD281 (TLR1)	GD2.F4	E660	40-9011-82	eBioscience
Monocolonal anti-mouse CD284 (TLR4)	SA15-21	Pe-Cy7	145408	Biolegend
Monoclonal anti-mouse CD289 (TLR9)	M9.D6	FITC	11-9093-82	eBioscience

Fluorometric Intracellular ROS	N/A	FITC	MAK144-1KT	Sigma Aldrich

3. Results

3.1 Gating strategy for gut and spleen cells

The same gating strategy was used for both the gut and the spleen. The first gate was selected for live cells by plotting FSC-A against Live/Dead V525 (Figure 4A, Figure 5A). Following, lymphocytes were selected by gating on size (Figure 4B, Figure 5B). Next, doublets were eliminated, and only single cells were gated by plotting the cell's area against height (Figure 4C, Figure 5C). CECs were selected by gating on TER119+CD71+ lymphocytes in both the gut and the spleen (Figure 4D, Figure 5D). From this population of cells, there was a gate placed around both CD45- and CD45+ TER119+CD71+ cells (Figure 4E, Figure 5E).

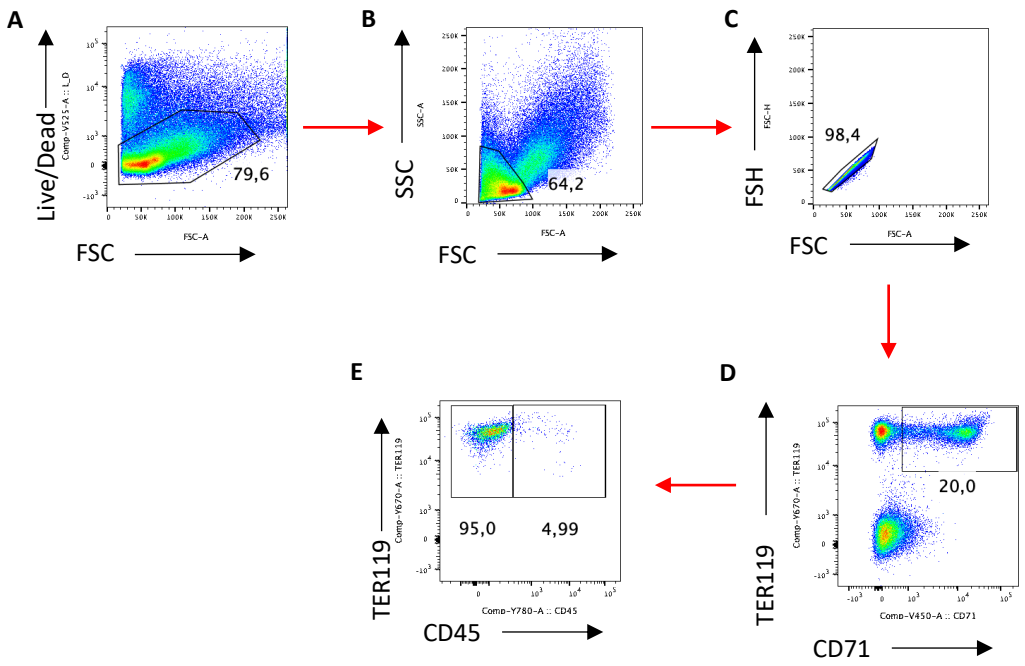

Figure 4: Gating Strategy for Gut Cells.

Cells were obtained from the small intestine and colon through single-cell isolation. Approximately 1,000,000 cells were plated and incubated with Live/Dead fixable Aqua (Life Technologies). The cells were then incubated with DCFDA for intracellular ROS staining. Next, cells were incubated with anti-CD71 (clone R17217), anti-TER119 (clone TER-119), anti-CD45 (clone 30-F11), and anti-VISTA (clone MIH63) antibodies. The voltage for forward and side scatter was set according to the BD Fortessa flow cytometer settings. The voltages for all listed markers were set based on the positioning of the positive and negative peaks and were kept consistent through all experiments. The gating approach was set as follows: dead cells were first excluded using a viability gate (A), lymphocytes were selected by gating the cells according to their size (B), the next gate was set to select single cells (C), CD71 was plotted against TER119, and a gate was set on the double-positive cells (D), finally, CD45 was plotted with TER119 to set a gate around CD45 negative and positive cells (E).

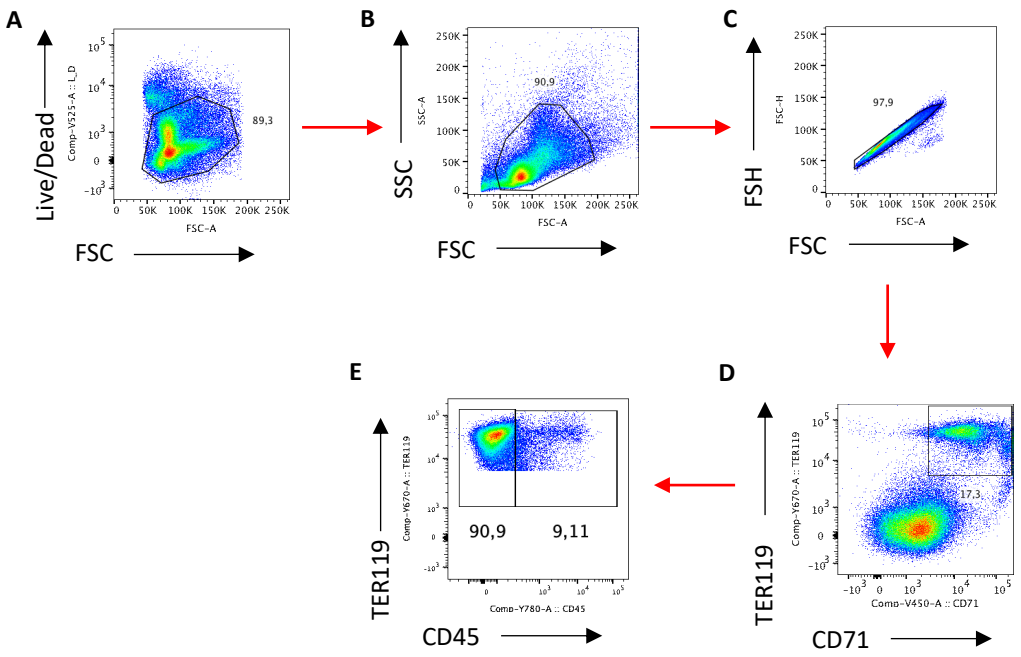

Figure 5: Gating Strategy for Spleen Cells.

Cells were obtained from the spleen through single-cell isolation. Approximately 1,000,000 cells were plated and incubated with Live/Dead fixable Aqua (Life Technologies). The cells were then incubated with DCFDA for intracellular ROS staining. Next, cells were incubated with anti-CD71 (clone R17217), anti-TER119 (clone TER-119), anti-CD45 (clone 30-F11), and anti-VISTA (clone MIH63) antibodies. The voltage for forward and side scatter was set according to the BD Fortessa flow cytometer settings. The voltages for all listed markers were set based on the positioning of the positive and negative peaks and were kept consistent through all experiments. The gating approach was set as follows: dead cells were first excluded using a viability gate (A), lymphocytes were selected by gating the cells according to their size (B), the next gate was set to select single cells (C), CD71 was plotted against TER119, and a gate was set on the double-positive cells (D), finally, CD45 was plotted with TER119 to set a gate around CD45 negative and positive cells (E).

3.2 AIM 1A

3.2.1 The spleen had higher percentages of CECs on days 3 and 6 relative to the gut

Representative plots were selected to visualize the CEC population in the gut and spleen at all time points (Figure 6A & 6B). On day 1 there were no significant differences in the percentage frequencies of CECs in the gut and the spleen, both groups averaging approximately ~15% CECs (Figure 6C). However, on day 3, the percentage of CECs in the spleen increased compared to the gut, resulting in a difference between the two tissues ($p<0.001$) (Figure 6C). This same trend was also observed on day 6, where CECs in the spleen were greater in comparison to the gut ($P<0.001$) (Figure 6C). As newborn mice develop, there is a need for increased erythropoiesis to produce adequate levels of erythrocytes to support the growing pup. The spleen is a key erythropoietic tissue in mice, specifically during stress Fields(84). This explains the increase of CECs in the spleen observed on days 3 and 6 relative to day 1 ($p<0.001$) (Figure 6C). In contrast, in the gut, there were no significant differences in CEC percentage at the recorded time points.

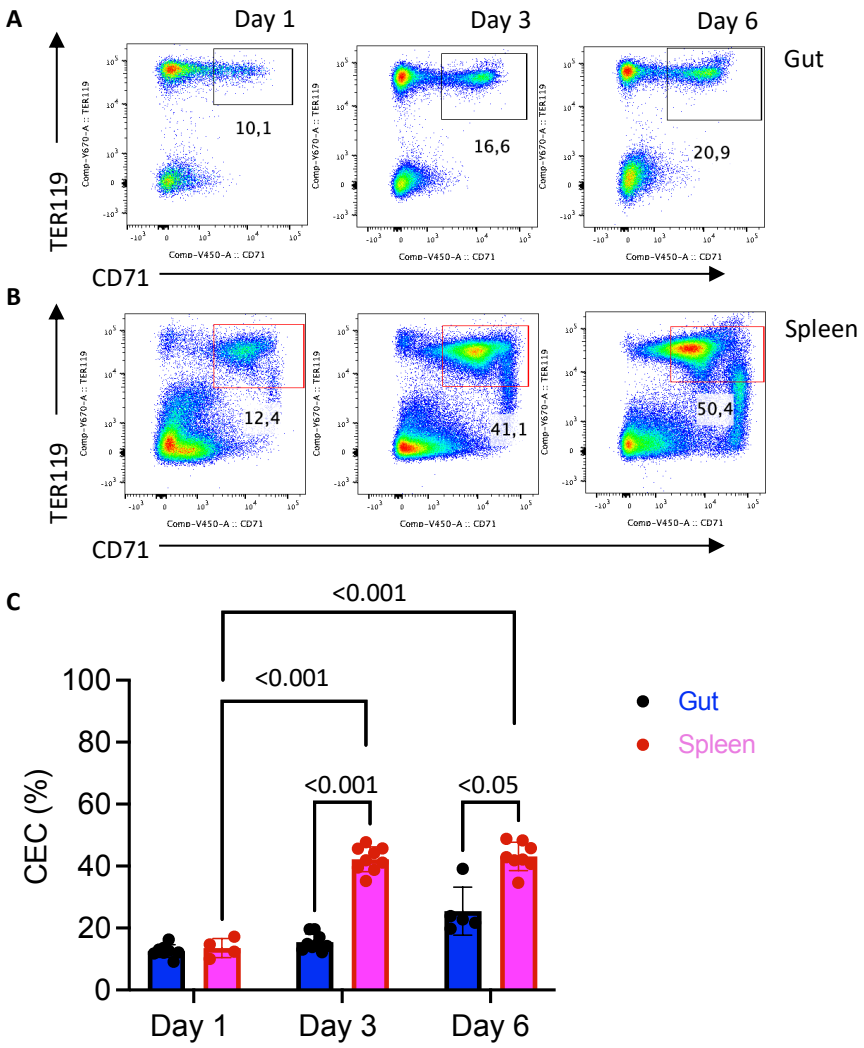

Figure 6: The spleen had significantly higher percentages of TER119⁺ CD71⁺ cells (CECs) on days 3 and 6 compared to the gut.

Cells were prepared as in Figures 4 and 5. (A) Representative plots for TER119⁺ CD71⁺ cells in the gut on days 1, 3 and 6. (B) Representative plots for TER119⁺ CD71⁺ cells in the spleen on days 1, 3 and 6. (C) On days 3 and 6, there were significantly higher percentages of CECs in the spleen compared to the gut ($p<0.05$). (C) On days 3 and 6 there were significant increases in the percentage of CECs in the spleen relative to day 1 ($p<0.001$). Results were analyzed with mixed effects model followed by Tukey's multiple comparisons test (n= 8 D1 Gut, n= 4 D1 Spleen, n= 8 D3 Gut, n= 9 D3 Spleen, n= 5 D6 Gut, n= 8 D6 Spleen. Shown are mean ± SEM). Data is presented from single experiments which have been repeated once. Sex of mice was not reported since it was not determined at euthanasia.

3.2.2 $CD45^+$ CECs from both the gut and the spleen have higher VISTA expression compared to $CD45^-$ CECs

Previously published data have shown that neonatal CECs express significant levels of VISTA (69). However, characterization dependent on the expression of CD45 on the surface of CECs had not been investigated. Representative plots were selected to visualize the $VISTA^+$ $CD45^-$ CEC and $VISTA^+$ $CD45^+$ CEC populations in the gut and spleen at all time points (Figure 7A & 7B). A negative control, the fluorescence minus one (FMO), was used to determine the positive gate for VISTA (Figure 7C). At all recorded time points in the gut, there were significantly higher percentages of $CD45^+$ CECs that expressed the VISTA receptor on their cell surface compared to $CD45^-$ CECs ($P<0.001$) (Figure 7D). This pattern was also observed in the spleen at all recorded time points ($p<0.001$). As mentioned, CD45 is found on all hematopoietic cells, excluding mature erythrocytes and platelets. This indicates that $CD45^-$ CECs are the mature subset of erythrocytes in comparison to $CD45^+$ CECs. Essentially, these data indicate that there are significantly higher percentages of immature CECs (expressing CD45) also expressing VISTA on their cell surface. Interestingly, on days 3 and 6, there were significantly higher percentages of $CD45^+$ CECs in the gut that expressed VISTA compared to $CD45^+$ CECs in the spleen ($p=0.0005$, $p=0.0465$ for day 3 and day 6, respectively) (Figure 7D). Similarly, on day 1, there was a significantly higher percentage of CD45- CECs in the gut that expressed VISTA compared to $CD45^-$ CECs in the spleen ($p>0.05$) (Figure 7D). These data indicate that CECs differentially express VISTA on their cell surface depending on the microenvironment.

In addition to analyzing the percentages of CECs that expressed VISTA on their cell surface, mean fluorescence intensity (MFI) was used to measure the relative amounts of VISTA on the

surface of CECs. MFI measurement indicates the intensity of marker on the surface of target cells and correlates with antigen amount, as opposed to the absence or presence of the marker that percentages capture. The FMO was used as a negative control for VISTA MFI in both the gut and the spleen (Figures 8A & 8B). Correspondingly, at all recorded time points, $CD45^+$ CECs expressed significantly higher levels of the VISTA receptor on their cell surface compared to CD45- CECs in the gut ($P<0.01$) (Figure 8C). This pattern was also observed in the spleen at all recorded time points ($p<0.001$). On day 3, $CD45^+$ CECs in the gut expressed significantly higher levels of VISTA compared to $CD45^+$ CECs from the spleen ($p<0.001$) (Figure 8C). Likewise, on day 1, CD45- CECs in the gut expressed significantly higher levels of VISTA compared to CD45- CECs in the spleen ($p<0.01$) (Figure 8C).

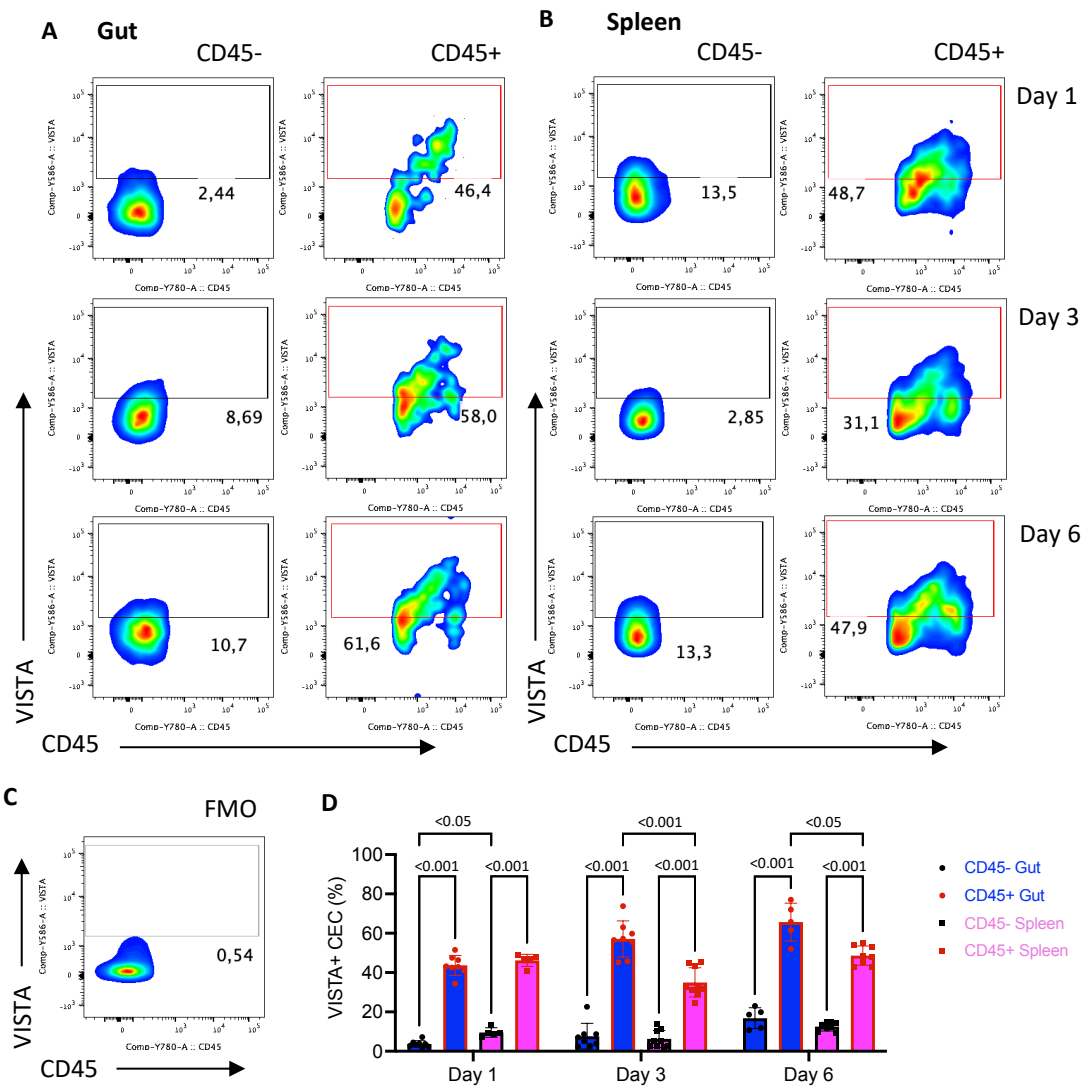

Figure 7: There were significantly higher percentages of CD45⁺ CECs that expressed VISTA in both the gut and spleen compared to CD45⁻ CECs.

Cells were prepared as in Figures 4 and 5. (A) Representative plots of VISTA⁺ CECs in the gut after either gating on CD45⁻ or CD45⁺. (B) Representative plots of VISTA⁺ CECs in the spleen after either gating on CD45⁻ or CD45⁺. (C) Representative plot of negative control for VISTA that was used to set the positive population gate. (D) At all time points, a significantly higher percentage of CD45⁺ CECs in both the gut and spleen expressed VISTA ($p < 0.05$). (D) On days 3 and 6, a significantly higher percentage of CD45⁺ CECs in the gut expressed VISTA compared to CD45⁺ CECs in the spleen ($p < 0.05$ for both comparisons). (D) On day 1, a significantly higher percentage of CD45⁻ CECs in the spleen expressed VISTA compared to CD45+ CECs in the gut ($p<0.05$). Results were analyzed with a mixed-effects model followed by Tukey's multiple comparisons test (n= 8 D1 Gut, n= 5 D1 Spleen, n= 8 D3 Gut, n= 9 D3 Spleen, n= 5 D6 Gut, n= 8

D6 Spleen. Shown are mean ± SEM). Data is presented from single experiments which have been repeated once. Sex of mice was not reported since it was not determined at euthanasia.

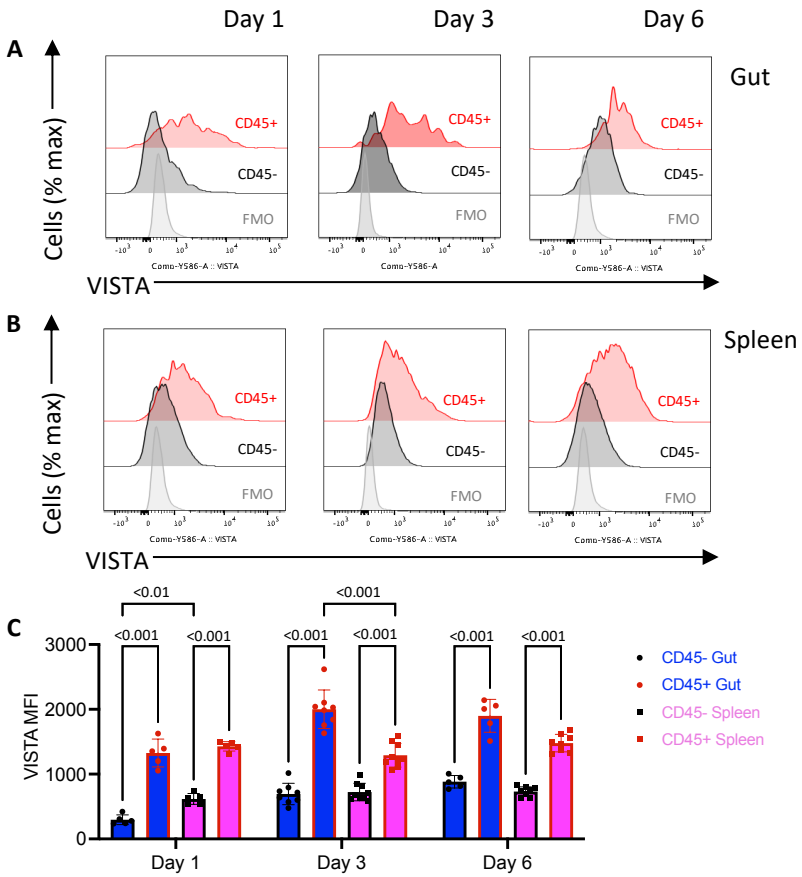

Figure 8: CD45⁺ CECs in both the gut and spleen expressed significantly higher levels of VISTA compared to CD45⁻ CECs.

Cells were prepared as in Figures 4 and 5. (A) Representative MFI plots for CD45⁻ and CD45⁺ CECs in the gut. Each sample was plotted against the negative control for VISTA, the FMO. (B) Representative MFI plots for CD45⁻ and CD45⁺ CECs in the spleen. Each sample was plotted against the negative control for VISTA, the FMO. (C) At all time points, CD45⁺ CECs expressed significantly higher levels of VISTA compared to CD45⁻ CECs, in both the gut and spleen ($p<0.05$). (C) On day 1, CD45⁻ CECs in the spleen expressed significantly higher levels of VISTA compared to CD45⁻ CECs in the gut ($p<0.01$). (C) On day 3, CD45⁺ CECs in the gut expressed significantly higher levels of VISTA compared to CD45+ CECs in the spleen ($p<0.001$). Results were analyzed with mixed-effects model followed by Tukey's multiple comparisons test (n= 5 D1 Gut, n= 5 D1 Spleen, n= 8 D3 Gut, n= 9 D3 Spleen, n= 5 D6 Gut, n= 8 D6 Spleen. Shown are mean ± SEM). Data is presented from single experiments which have been repeated once. Sex of mice was not reported since it was not determined at euthanasia.

3.2.3 $CD45^+$ CECs in both the gut and spleen expressed higher levels of ROS compared to $CD45^-$ CECs

MFI was used to measure the relative amounts of reactive oxygen species (ROS) on the surface of CECs. An FMO was used as a negative control for ROS MFI in both the gut and the spleen (Figures 9A & 9B). At all recorded time points, $CD45^+$ CECs expressed significantly higher levels of ROS intracellularly compared to $CD45^-$ CECs in the gut ($p<0.05$) (Figure 9C). This pattern was also observed in the spleen at all recorded time points ($p<0.001$) (Figure 9C). On day 3, $CD45^-$ CECs in the spleen expressed significantly higher levels of ROS compared to $CD45^-$ CECs from the gut ($p<0.05$) (Figure 9C). Likewise, on day 6, $CD45^-$ CECs in the spleen expressed higher levels of ROS compared to $CD45^-$ CECs in the gut ($p<0.01$) (Figure 9C).

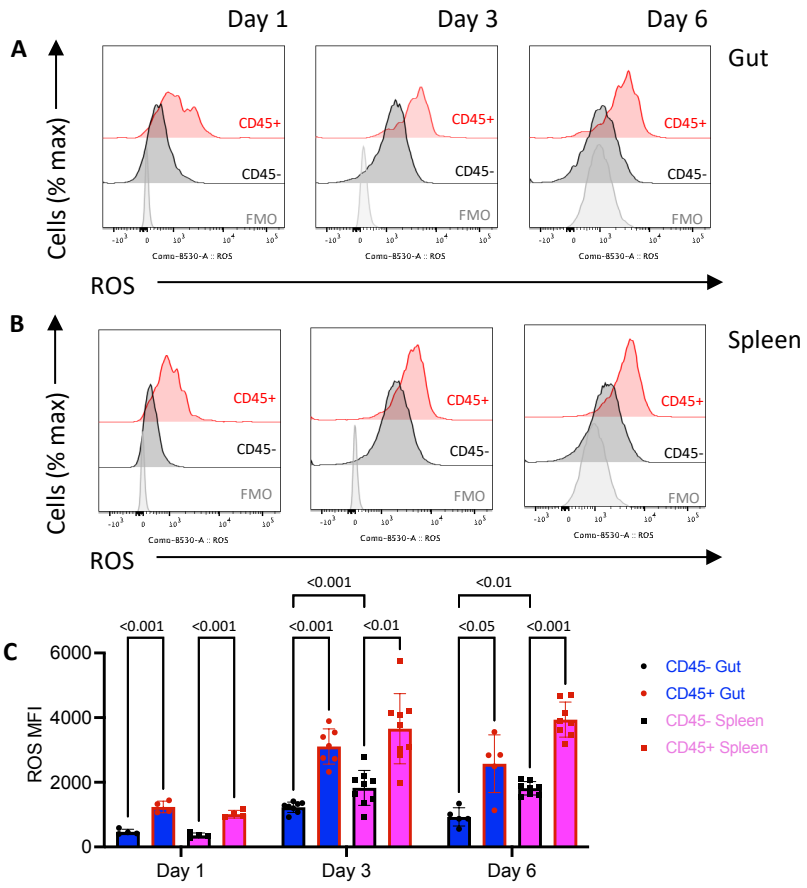

Figure 9: CD45$^+$ CECs in both the gut and spleen expressed significantly higher levels of ROS compared to CD45$^-$ CECs.

Cells were prepared as in Figures 4 and 5. (A) Representative MFI plots for CD45$^-$ and CD45$^+$ CECs in the gut. Each sample was plotted against the negative control for ROS, the FMO. (B) Representative MFI plots for CD45$^-$ and CD45$^+$ CECs in the spleen. Each sample was plotted against the negative control for ROS, the FMO. (C) At all time points, CD45$^+$ CECs in both the gut and spleen expressed significantly higher percentages of ROS ($p<0.05$). (C) On days 3 and 6, CD45$^-$ CECs in the spleen expressed significantly higher levels of ROS compared to CD45$^-$ CECs in the gut ($p<0.05$). Results were analyzed with mixed-effects model followed by Tukey's multiple comparisons test (n= 4 D1 Gut, n= 4 D1 Spleen, n= 8 D3 Gut, n= 9 D3 Spleen, n= 5 D6 Gut, n= 8 D6 Spleen. Shown are mean ± SEM). Data is presented from single experiments which have been repeated once. Sex of mice was not reported since it was not determined at euthanasia.

3.2.4 $CD45^+$ CECs in both the gut and spleen expressed higher levels of TGF-β compared to $CD45^-$ CECs

Day 1 samples were not collected for TGF-β and arginase-1 expression due to the lack of sufficient cell collection that is required during intracellular staining. MFI was used to measure the relative amounts of TGF-β in the cytosol of CECs. An FMO was used as a negative control for TGF-β MFI in both the gut and the spleen (Figures 10A & 10B). At all recorded time points, $CD45^+$ CECs expressed significantly higher levels of TGF-β in the cytosol compared to $CD45^-$ CECs in the gut ($p<0.001$) (Figure 10C). In contrast, in the spleen, $CD45^+$ CECs had significantly higher levels of TGF-β compared to $CD45^-$ CECs at day 3 only ($p<0.001$) (Figure 10C). At all recorded time points, $CD45^+$ CECs from the gut expressed significantly higher levels of TGF-β compared to $CD45^+$ CECs from the spleen ($p<0.01$) (Figure 10C).

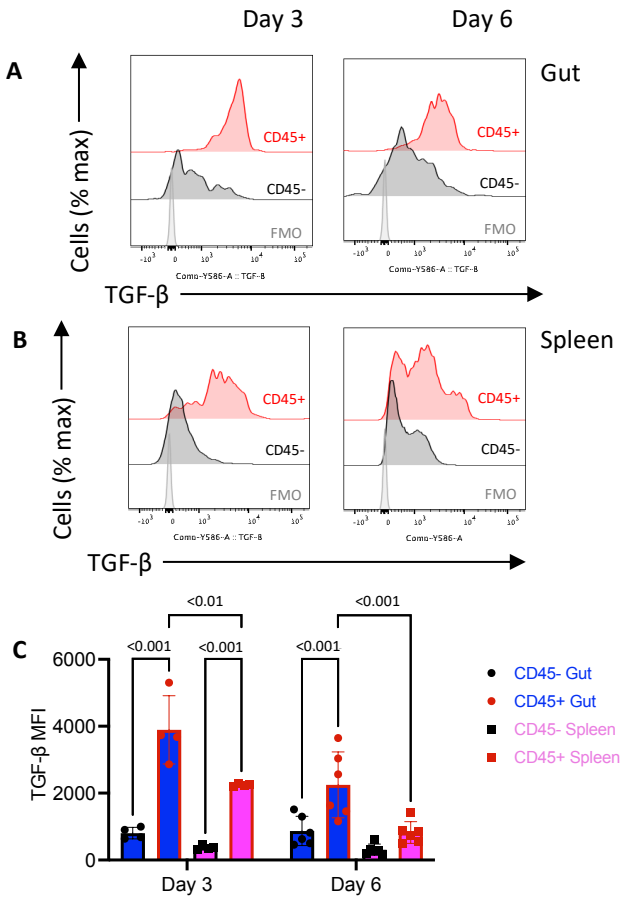

Figure 10: CD45⁺ CECs in both the gut and spleen expressed significantly higher levels of TGF-β compared to CD45⁻ CECs.

Cells were obtained as in Figures 4 and 5. (A) Representative MFI plots for CD45⁻ and CD45+ CECs in the gut. Each sample was plotted against the negative control for TGF-β, the FMO. (B) Representative MFI plots for CD45⁻ and CD45⁺ CECs in the spleen. Each sample was plotted against the negative control for TGF-β, the FMO. (C) On day 3, CD45⁺ CECs in both the gut and spleen expressed significantly higher levels of TGF-β ($p<0.05$). (C) On day 6, CD45⁺ CECs from the gut expressed significantly higher levels of TGF-β compared to CD45- CECs ($p<0.001$). (C) At all time points, CD45⁺ CECs from the gut expressed significantly higher levels of TGF-β compared to CD45⁺ CECs from the spleen ($p < 0.05$ for all comparisons). Results were analyzed with mixed effects model followed by Tukey's multiple comparisons test. Samples were not collected at the day 1 time point due to the lack of sufficient cell count in the tissues needed for intracellular staining (n= 4 D3 Gut, n= 4 D3 Spleen, n= 6 D6 Gut, n= 6 D6 Spleen. Shown are mean ± SEM). Data is presented from single experiments which have been repeated once. Sex of mice was not reported since it was not determined at euthanasia.

3.2.5 $CD45^+$ CECs in both the gut and spleen expressed higher levels of arginase-1 compared to $CD45^-$ CECs

MFI was used to measure the relative amount of arginase-1 in the cytosol of CECs. An FMO was used as a negative control for arginase-1 MFI in both the gut and the spleen (Figures 11A & 11B). At all recorded time points, $CD45^+$ CECs expressed significantly higher levels of arginase-1 in the cytosol compared to $CD45^-$ CECs in the gut ($p<0.001$) (Figure 11C). This pattern was also observed in the spleen at all recorded time points ($p<0.01$) (Figure 11C). Moreover, at all recorded time points, $CD45^+$ CECs from the gut expressed higher levels of arginase-1 compared to $CD45^+$ CECs from the spleen ($p<0.001$) (Figure 11C). On day 3, $CD45^-$ CECs from the gut expressed significantly higher levels of arginase-1 compared to $CD45^-$ CECs from the spleen ($p<0.05$) (Figure 11C).

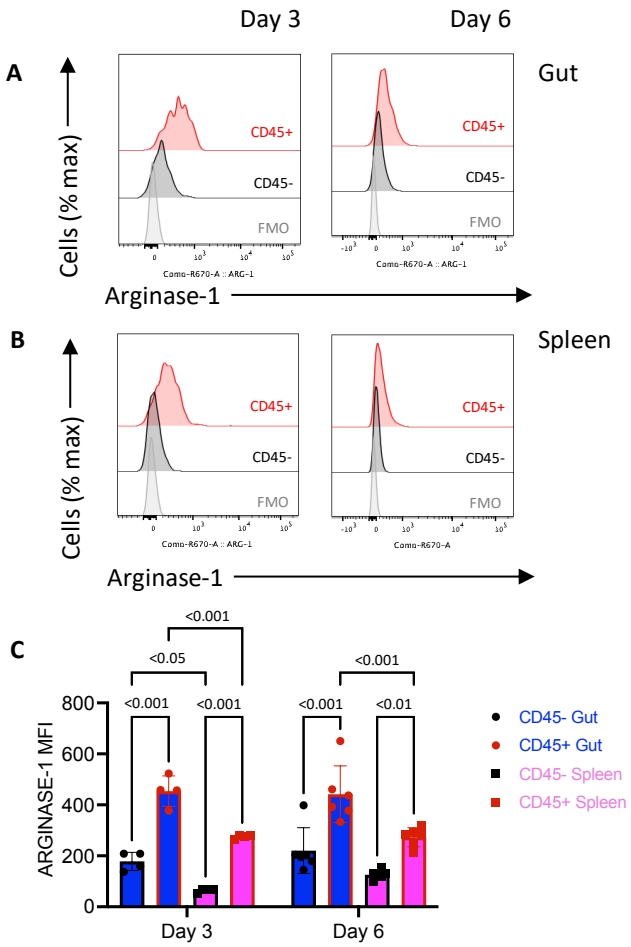

Figure 11: CD45$^+$ CECs in both the gut and spleen expressed significantly higher levels of arginase-1 compared to CD45$^-$ CECs.

Cells were prepared as in Figures 4 and 5. (A) Representative MFI plots for CD45$^-$ and CD45$^+$ CECs in the gut. Each sample was plotted against the negative control for arginase-1, the FMO. (B) Representative MFI plots for CD45$^-$ and CD45$^+$ CECs in the spleen. Each sample was plotted against the negative control for arginase-1, the FMO. (C) At all time points, CD45$^+$ CECs in both the gut and spleen expressed significantly higher levels of arginase-1 ($p<0.05$). (C) On day 3, CD45$^-$ CECs in the gut expressed significantly higher levels of arginase-1 compared to CD45$^-$ CECs in the spleen ($p<0.05$). (C) At all time points, CD45$^+$ CECs in the gut expressed higher levels of arginase-1 compared to CD45+ CECs in the spleen ($p<0.05$). Results were analyzed with mixed effects model followed by Tukey's multiple comparisons test. Samples were not collected at the day 1 timepoint due to the lack of sufficient cell count in the tissues needed for intracellular staining (n= 4 D3 Gut, n= 4 D3 Spleen, n= 6 D6 Gut, n= 6 D6 Spleen. Shown are mean ± SEM). Data is presented from single experiments which have been repeated once. Sex of mice was not reported since it was not determined at euthanasia.

3.3 AIM 1B

3.3.1 SPF mice had higher percentages of CECs on day 1 only, in the gut and spleen, compared to GF mice

Representative plots were selected to visualize the CEC population in the gut and spleen of SPF and GF mice at all time points (Figure 12A & 12B). In the gut on day 1, SPF mice had significantly higher percentages of CECs relative to GF mice ($p<0.05$) (Figure 12C). Similarly, in the spleen on day 1, SPF mice had significantly higher percentages of CECs relative to GF mice ($p<0.05$) (Figure 12C). On days 3 and 6, there were no significant differences in CEC percentage between SPF and GF mice, in both the gut and spleen (Figure 12C).

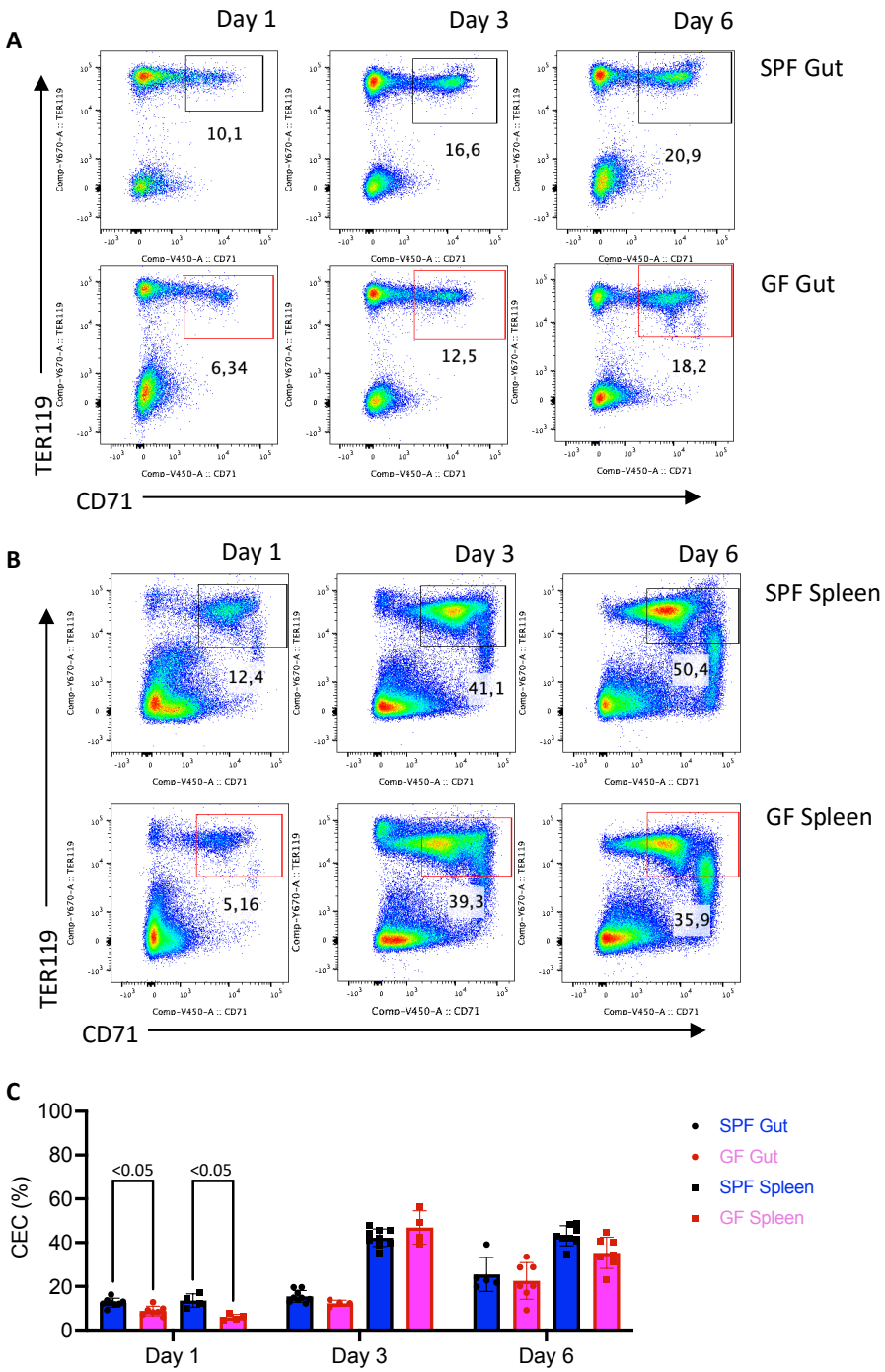

Figure 12: SPF mice had significantly higher percentages of CECs on day 1 only, in the gut and spleen, compared to GF mice.

Cells were prepared as in Figures 4 and 5. (A) Representative plots for $TER119^+$ $CD71^+$ cells in the gut of SPF and GF mice on days 1, 3 and 6. (B) Representative plots for $TER119^+$ $CD71^+$ cells in the spleen of SPF and GF mice on days 1, 3 and 6. (C) On day 1, SPF mice had higher percentages of CECs in the gut compared to GF mice ($p<0.05$). (C) On day 1, SPF mice had

higher percentages of CECs in the spleen compared to GF mice ($p<0.05$). Results were analyzed with mixed-effects model followed by Tukey's multiple comparisons test (n= 8 D1 SPF Gut, n= 7 D1 GF Gut, n= 4 D1 SPF Spleen, n= 4 D1 GF Spleen, n= 8 D3 SPF Gut, n= 4 D3 GF Gut, n= 9 D3 SPF Spleen, n= 4 D3 GF Spleen, n= 5 D6 SPF Gut, n= 7 D6 GF Gut, n= 8 D6 SPF Spleen, n= 7 D6 GF Spleen. Shown are mean ± SEM). Data is presented from single experiments which have been repeated once. Sex of mice was not reported since it was not determined at euthanasia.

3.3.2 CECs from the guts and spleens of SPF mice exhibit greater VISTA expression relative to CECs from GF mice

Representative plots were selected to visualize the $VISTA^+$ $CD45^-$ CEC and $VISTA^+$ $CD45^+$ CEC populations in the guts of SPF and GF mice at all time points (Figure 13A & 13B). Like the gut, representative plots were selected to visualize the $VISTA^+$ $CD45^-$ CEC and $VISTA^+$ $CD45^+$ CEC populations in the spleen of SPF and GF mice at all time points (Figure 14A & 14B). A negative control, the FMO, was used to determine the positive gate for VISTA (Figures 13C & 14C). MFI was used to measure the relative amounts of VISTA on the surface of CECs from SPF and GF mice. The VISTA FMO was used as a negative control for VISTA MFI in both the gut and the spleen of SPF and GF mice (Figure 15A & 15B and Figure 16A & 16B).

In the gut on day 3, there were significantly higher percentages of $CD45^+$ CECs that expressed VISTA in SPF mice relative to GF mice ($p<0.001$) (Figure 13D). Moreover, on day 3, both $CD45^-$ and $CD45^+$ CECs from the guts of SPF mice expressed higher levels of VISTA on their cell surface relative to their GF counterparts ($p<0.05$) (Figure 15C). On day 6, there were significantly higher percentages of gut $CD45^-$ CECs that expressed VISTA in SPF mice relative to GF mice ($p=0.0346$) (Figure 13A). Correspondingly, on day 6, these gut $CD45^-$ CECs from SPF mice expressed significantly higher levels of VISTA relative to those from GF mice (0.0141) (Figure 15C). Interestingly, on day 1 $CD45^-$ CECs from GF mice expressed significantly higher levels of VISTA relative to $CD45^-$ CECs from SPF mice ($p<0.05$) (Figure 15C).

In the spleen, on day 3, there were higher percentages of $CD45^+$ CECs that expressed VISTA in SPF mice relative to GF mice ($p<0.05$) (Figure 14D). On day 3, both $CD45^-$ and $CD45^+$ CECs from

SPF mice expressed higher levels of VISTA relative to $CD45^-$ and $CD45^+$ CECs from GF mice ($p<0.05$) (Figure 16C). On day 6, there were higher percentages of both $CD45^-$ and $CD45^+$ CECs that expressed Vista from the spleens of SPF mice relative to their GF counterparts ($p<0.001$) (Figure 14D). Correspondingly, on day 6, these $CD45^-$ and $CD45^+$ CECs from SPF mice expressed higher levels of VISTA relative to $CD45^-$ and $CD45^+$ CECs from GF mice ($p<0.05$) (Figure 16C).

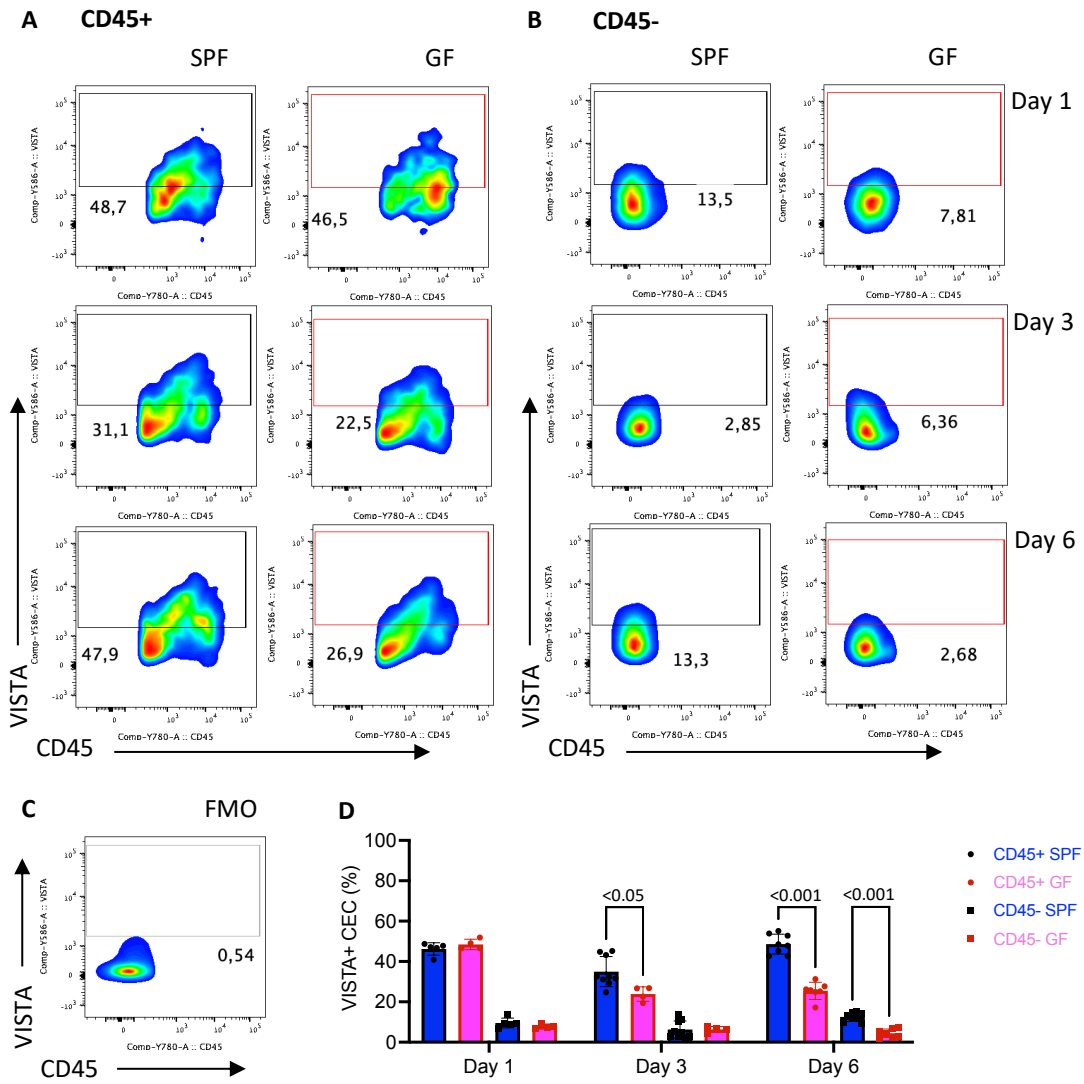

Figure 13: Significantly higher percentages of CD45⁺ CECs from the guts of SPF mice expressed VISTA compared to those from GF counterparts on days 3 and 6.

Cells were prepared as in Figures 4 and 5. (A) Representative plots of VISTA⁺ CD45⁺ CECs from the guts of SPF and GF mice. (B) Representative plots of VISTA⁺ CD45⁻ CECs from the guts of SPF and GF mice. (C) Representative plot of negative control for VISTA that was used to set the positive population gate. (D) On day 3, significantly higher percentages of CD45⁺ CECs from SPF mice expressed more VISTA compared to CD45⁺ CECs from GF mice ($p<0.05$). (D) On day 6, there were significantly higher percentages of both CD45⁻ and CD45⁺ CECs that expressed VISTA from SPF mice compared to GF counterparts ($p<0.05$). Results were analyzed with mixed-effects model followed by Tukey's multiple comparisons test (n= 8 D1 SPF Gut, n= 6 D1 GF Gut, n= 8 D3 SPF Gut, n= 4 D3 GF Gut, n= 5 D6 SPF Gut, n= 7 D6 GF Gut. Shown are mean ± SEM). Data is presented from single experiments which have been repeated once. Sex of mice was not reported since it was not determined at euthanasia.

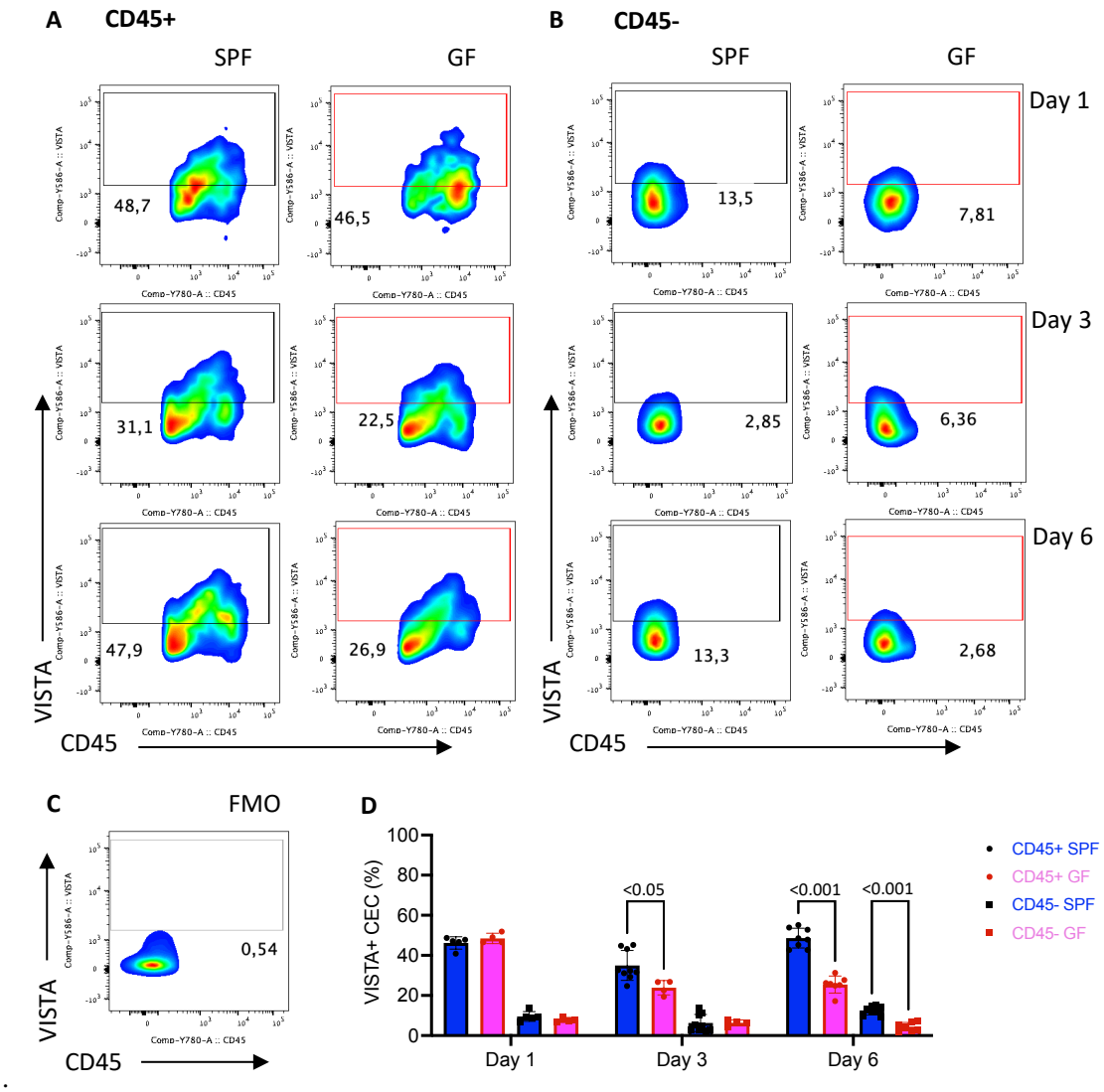

Figure 14: Significantly higher percentages of CD45⁺ CECs from spleens from SPF mice expressed VISTA compared to those from GF counterparts on days 3 and 6.

Cells were prepared as in Figures 4 and 5. (A) Representative plots of VISTA⁺ CD45⁺ CECs from the spleens of SPF and GF mice. (B) Representative plots of VISTA⁺ CD45⁻ CECs from the spleens of SPF and GF mice. (C) Representative plot of negative control for VISTA that was used to set the positive population gate. (D) On day 3, significantly higher percentages of CD45+ CECs from SPF mice expressed VISTA compared to CD45⁺ CECs from GF mice ($p = 0.0183$). (D) On day 6, significantly higher percentages of both CD45⁻ and CD45⁺ CECs from SPF mice expressed VISTA compared with those from GF counterparts ($p<0.001$). Results were analyzed with mixed-effects model followed by Tukey's multiple comparisons test (n= 5 D1 SPF Spleen, n= 4 D1 GF Spleen, n= 9 D3 SPF Spleen, n= 4 D3 GF Spleen, n= 8 D6 SPF Spleen, n= 7 D6 GF Spleen. Shown are mean ± SEM). Data is presented from single experiments which have been repeated once. The sex of the mice was not reported since it is not determinable in young pups.

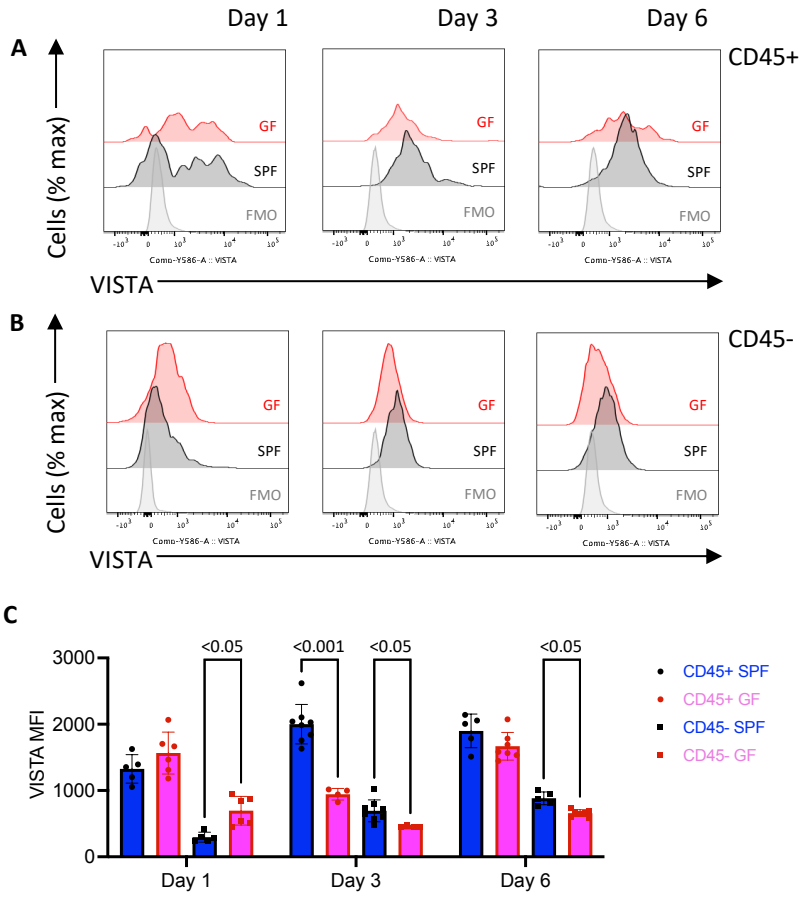

Figure 15: CD45$^-$ and CD45$^+$ CECs from the guts of SPF mice expressed significantly higher levels of VISTA compared to CD45$^-$ and CD45$^+$ CECs from the guts of GF mice on day 3.

Cells were prepared as in Figures 4 and 5. (A) Representative MFI plots for CD45$^+$ CECs from the guts of SPF and GF mice. Each sample was plotted against the negative control for VISTA, the FMO. (B) Representative MFI plots for CD45$^-$ CECs from the guts of SPF and GF mice. Each sample was plotted against the negative control for VISTA, the FMO. (C) On day 1, CD45$^-$ CECs from the guts of GF mice expressed significantly higher levels of VISTA compared to CD45$^-$ CECs from the guts of SPF mice ($p<0.05$). (C) On day 3, CD45$^+$ CECs from the guts of SPF mice expressed significantly higher levels of VISTA compared to CD45$^+$ CECs from GF guts ($p<0.05$). (C) On day 6, CD45$^-$ CECs from the guts of SPF mice expressed significantly higher levels of VISTA compared to CD45$^-$ CECs from GF guts ($p<0.05$). Results were analyzed with mixed effects model followed by Tukey's multiple comparisons test (n= 5 D1 SPF Gut, n= 6 D1 GF Gut, n= 8 D3 SPF Gut, n= 4 D3 GF Gut, n= 5 D6 SPF Gut, n= 7 D6 GF Gut. Shown are mean ± SEM). Data is presented from single experiments which have been repeated once. Sex of mice was not reported since it was not determined at euthanasia.

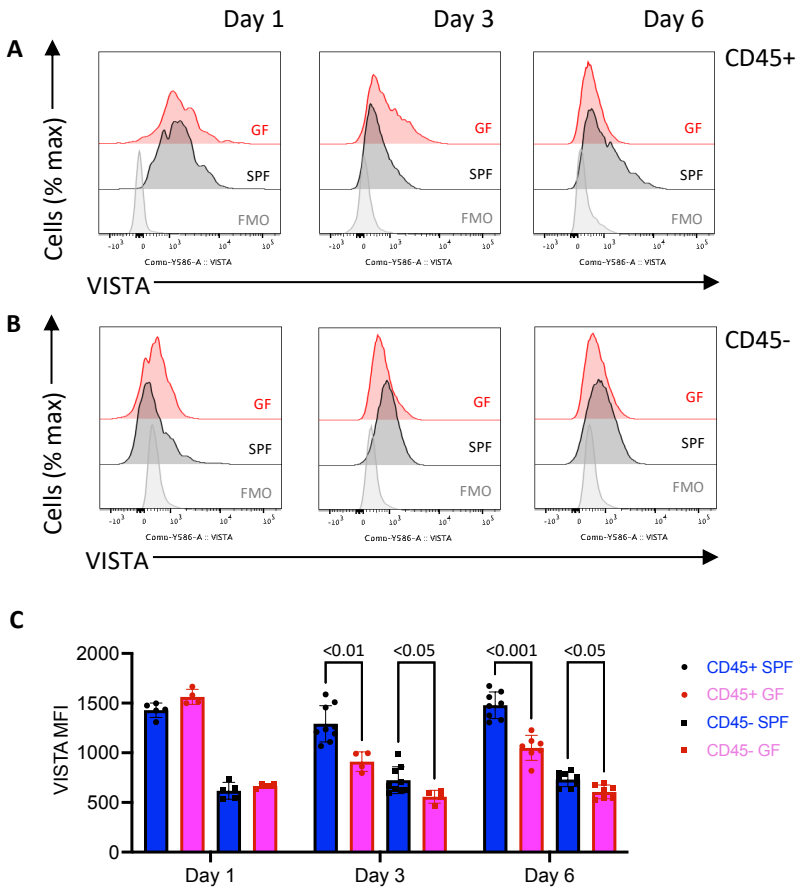

Figure 16: CD45$^-$ and CD45$^+$ CECs from the spleens of SPF mice expressed significantly higher levels of VISTA compared to CD45$^-$ and CD45$^+$ CECs from spleens of GF mice on days 3 and 6.

Cells were prepared as in Figures 4 and 5. (A) Representative MFI plots for CD45$^+$ CECs from the spleens of SPF and GF mice. Each sample was plotted against the negative control for VISTA, the FMO. (B) Representative MFI plots for CD45$^-$ CECs from the spleens of SPF and GF mice. Each sample was plotted against the negative control for VISTA, the FMO. (C) On days 3 and 6, both CD45$^-$ and CD45$^+$ CECs from the spleens of SPF mice expressed higher levels of VISTA compared to those from GF counterparts ($p<0.05$). Results were analyzed with mixed effects model followed by Tukey's multiple comparisons test (n= 5 D1 SPF Spleen, n= 4 D1 GF Spleen, n= 9 D3 SPF Spleen, n= 4 D3 GF Spleen, n= 8 D6 SPF Spleen, n= 7 D6 GF Spleen. Shown are mean ± SEM). Data is presented from single experiments which have been repeated once. Sex of mice was not reported since it was not determined at euthanasia.

3.3.3 $CD45^+$ CECs from the guts and spleens of SPF mice expressed higher levels of ROS compared to $CD45^+$ CECs from GF mice

MFI was used to measure the relative amount of ROS on the surface of CECs. An FMO was used as a negative control for ROS MFI in gut CECs (Figures 14A & 14B). In the gut on day 1, both $CD45^-$ and $CD45^+$ CECs from SPF mice expressed significantly higher levels of ROS relative to $CD45^-$ and $CD45^+$ CECs from GF mice ($p<0.05$) (Figure 17C). On day 3 there were no significant differences in ROS expression. On day 6, $CD45^+$ CECs from SPF mice expressed higher levels of ROS compared to $CD45^+$ CECs from GF mice ($p<0.05$) (Figure 17C). However, there were no significant differences in ROS expression in gut $CD45^-$ CECs from SPF and GF mice (Figure 17C).

An FMO was used as a negative control for ROS MFI in spleen CECs (Figures 18A & 18B). In the spleen on day 1, there were no significant differences in ROS expression between SPF and GF mice. Interestingly, on day 3, $CD45^-$ CECs from GF mice expressed significantly higher levels of ROS relative to $CD45^-$ CECs from SPF mice ($p<0.05$) (Figure 18C). In contrast, on day 6, both $CD45^-$ and $CD45^+$ CECs from SPF mice expressed higher levels of ROS relative to $CD45^-$ and $CD45^+$ CECs from GF mice ($p<0.001$) (Figure 18C).

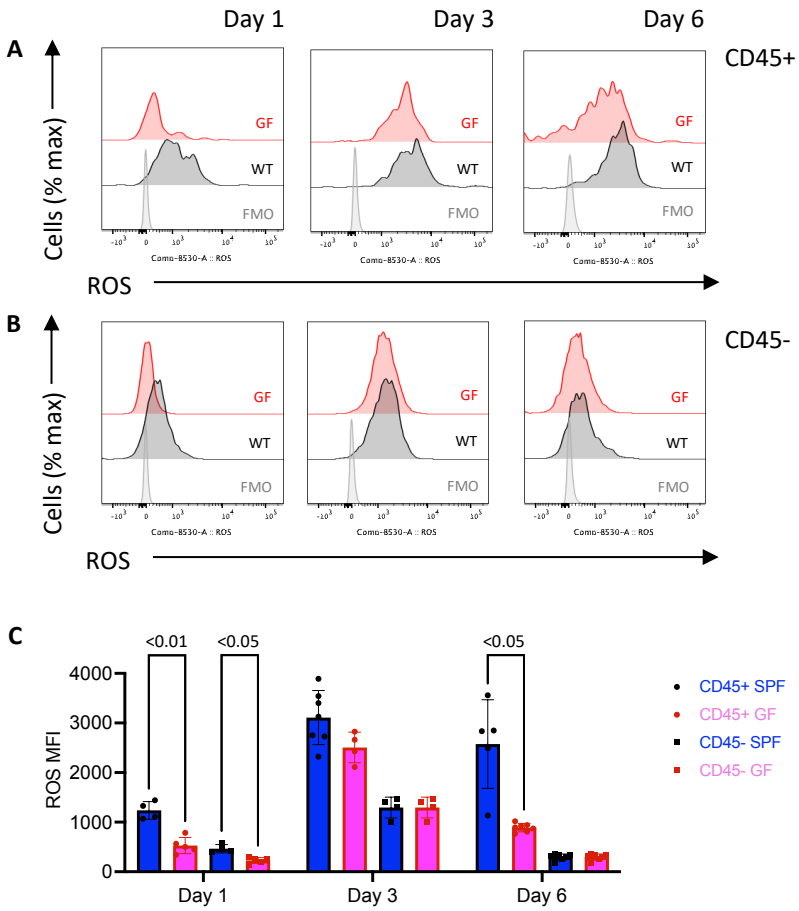

Figure 17: CD45⁺ CECs from the guts of SPF mice expressed significantly higher levels of ROS compared to CD45⁺ CECs from GF guts on days 1 and 6.

Cells were prepared as in Figures 4 and 5. (A) Representative MFI plots for CD45⁺ CECs from the guts of SPF and GF mice. Each sample is plotted against the negative control for ROS, the FMO. (B) Representative MFI plots for CD45⁻ CECs from the guts of SPF and GF mice. Each sample is plotted against the negative control for ROS, the FMO. (C) On day 1, both CD45⁻ and CD45⁺ CECs from the guts of SPF mice expressed significantly higher levels of ROS ($p<0.05$). (C) On day 6, CD45⁺ CECs from the gut of SPF mice expressed significantly higher levels of ROS compared with gut CD45⁺ CECs from GF mice ($p<0.05$). Results were analyzed with mixed effects model followed by Tukey's multiple comparisons test (n= 4 D1 SPF Gut, n= 5 D1 GF Gut, n= 7 D3 SPF Gut, n= 4 D3 GF Gut, n= 5 D6 SPF Gut, n= 7 D6 GF Gut. Shown are mean ± SEM). Data is presented from single experiments which have been repeated once. Sex of mice was not reported since it was not determined at euthanasia.

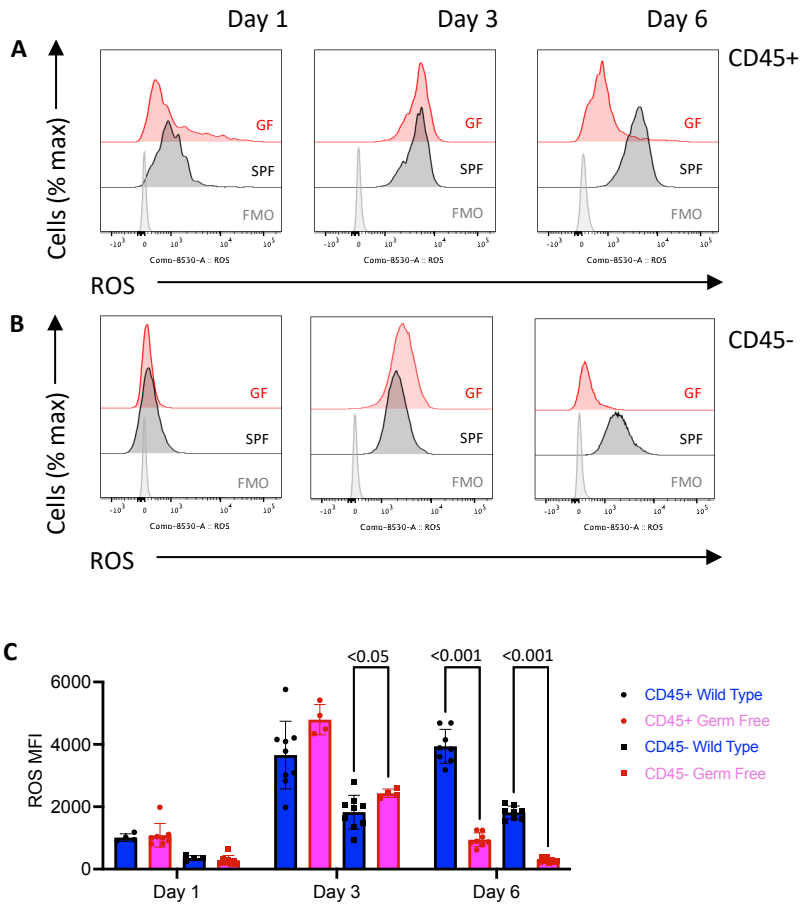

Figure 18: CD45$^+$ and CD45$^-$ CECs from the spleens of SPF mice expressed significantly higher levels of ROS compared to CD45$^+$ CECs from the spleens of GF mice on day 6.

Cells were prepared as in Figures 4 and 5. (A) Representative MFI plots for CD45$^+$ CECs from the spleens of SPF and GF mice. Each sample was plotted against the negative control for ROS, the FMO. (B) Representative MFI plots for CD45$^-$ CECs from the spleens of SPF and GF mice. Each sample was plotted against the negative control for ROS, the FMO. (C) On day 3, CD45$^-$ CECs from the spleens of GF mice expressed significantly higher levels of ROS ($p<0.05$). (C) On day 6, both CD45$^-$ and CD45$^+$ CECs from the spleens of SPF mice expressed significantly higher levels of ROS ($p<0.05$). Results were analyzed with mixed effects model followed by Tukey's multiple comparisons test (n= 4 D1 SPF Spleen, n= 8 D1 GF Spleen, n= 9 D3 SPF Spleen, n= 4 D3 GF Spleen, n= 8 D6 SPF Spleen, n= 8 D6 GF Spleen. Shown are mean ± SEM).
Data is presented from single experiments which have been repeated once. Sex of mice was not reported since it was not determined at euthanasia.

3.3.4 $CD45^+$ CECs from the guts and spleens of SPF mice expressed higher levels of TGF-β compared to $CD45^+$ CECs from GF mice

Day 1 samples were not collected for TGF-β and arginase-1 expression due to the lack of sufficient cell collection that is required during intracellular staining. MFI was used to measure the relative amount of TGF-β in the cytosol of CECs. An FMO was used as a negative control for TGF-β MFI in the cells from the guts of SPF and GF mice (Figures 19A & 19B). In the gut, on day 3, $CD45^+$ CECs from SPF mice expressed higher levels of TGF-β relative to $CD45^+$ CECs from GF mice ($p<0.001$) (Figure 19C). This same pattern was observed on day 6 in the gut ($p<0.05$) (Figure 19C).

An FMO was used as a negative control for TGF-β MFI in cells from the spleens of SPF and GF mice (Figures 20A & 20B). In the spleen, at day 3, $CD45^+$ CECs from SPF mice expressed significantly higher levels of TGF-β relative to $CD45^+$ CECs from GF mice ($p<0.001$) (Figure 20C). On day 6, the opposite pattern was observed in the spleen: $CD45^+$ CECs from GF mice expressed higher levels of TGF-β relative to $CD45^+$ CECs from SPF mice ($p<0.001$) (Figure 20C).

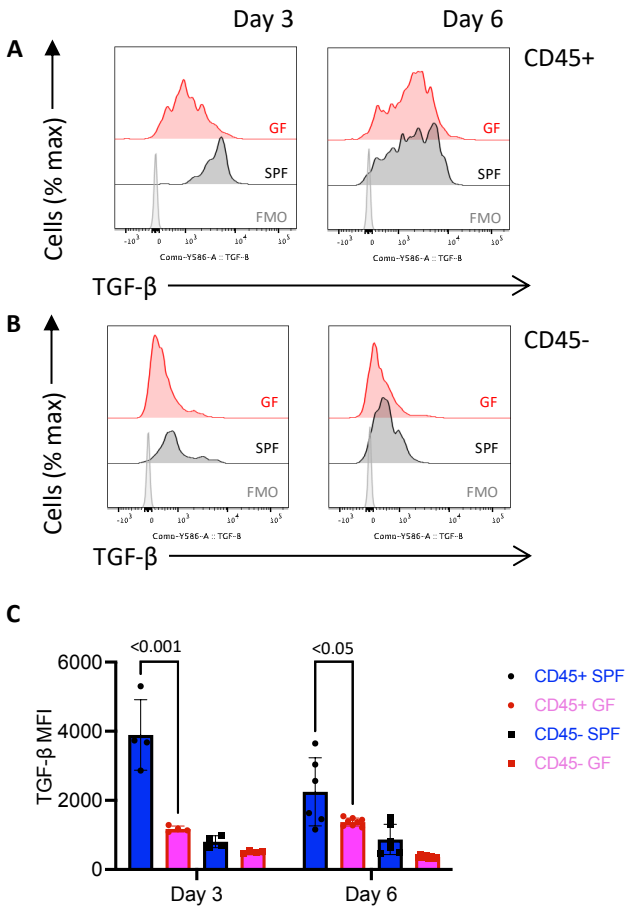

Figure 19: CD45⁺ CECs from the guts of SPF mice expressed significantly higher levels of TGF-β compared to CD45⁺ CECs from GF guts on days 3 and 6.

Cells were prepared as in Figures 4 and 5. (A) Representative MFI plots for CD45⁺ CECs from the guts of SPF and GF mice. Each sample was plotted against the negative control for TGF-β, the FMO. (B) Representative MFI plots for CD45⁻ CECs from the guts of SPF and GF mice. Each sample was plotted against the negative control for TGF-β, the FMO. (C) At all time points, CD45⁺ CECs from the guts of SPF mice expressed significantly higher levels of TGF-β compared to CD45⁺ CECs from GF guts ($p<0.05$). Samples were not collected at the day 1 time point due to the lack of sufficient cell count in the tissues needed for intracellular staining. Results were analyzed with mixed effects model followed by Tukey's multiple comparisons test (n= 4 D3 SPF Gut, n= 4 D3 GF Gut, n= 6 D6 SPF Gut, n= 6 D6 GF Gut. Shown are mean ± SEM). Data is presented from single experiments which have been repeated once. Sex of mice was not reported since it was not determined at euthanasia.

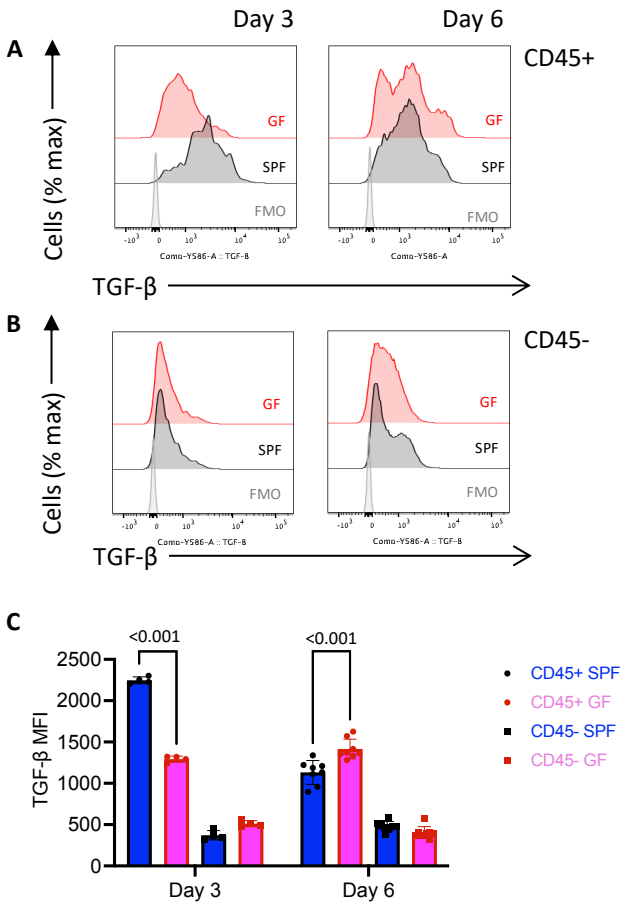

Figure 20: CD45⁺ CECs from the spleens of SPF mice expressed significantly higher levels of TGF-β compared to CD45⁺ CECs from the spleens of GF mice on day 3.

Cells were prepared as in Figures 4 and 5. (A) Representative MFI plots for CD45⁺ CECs from the spleens of SPF and GF mice. Each sample was plotted against the negative control for TGF-β, the FMO. (B) Representative MFI plots for CD45⁻ CECs from the spleens of SPF and GF mice. Each sample was plotted against the negative control for TGF-β, the FMO. (C) On day 3, CD45⁺ CECs from spleens of SPF mice expressed significantly higher levels of TGF-β compared to CD45⁺ CECs from spleens of GF mice ($p<0.001$). (C) On day 6, CD45+ CECs from the spleens of SPF mice expressed significantly lower levels of TGF-β compared to CD45⁺ CECs from spleens from GF mice ($p<0.001$). Samples were not collected at the day 1 time point due to the lack of sufficient cell count in the tissues needed for intracellular staining. Results were analyzed with mixed-effects model followed by Tukey's multiple comparisons test (n= 4 D3 SPF Spleen, n= 4 D3 GF Spleen, n= 8 D6 WSPF Spleen, n= 8 D6 GF Spleen. Shown are mean ± SEM). Data is presented from single experiments which have been repeated once. Sex of mice was not reported since it was not determined at euthanasia.

3.3.5 CECs from the guts and spleens of SPF mice expressed higher levels of arginase-1 compared to GF mice

MFI was used to measure the relative amount of arginase-1 in the cytosol of CECs. An FMO was used as a negative control for arginase-1 MFI (Figures 21A & 21B). In the gut, at day 3, both $CD45^-$ and $CD45^+$ CECs from SPF mice expressed significantly higher levels of arginase-1 relative to $CD45^-$ and $CD45^+$ CECs from GF mice ($p<0.01$) (Figure 21C). This same pattern was observed on day 6 in the gut ($p<0.05$) (Figure 21C).

An FMO was used as a negative control for arginase-1 MFI in cells from spleens of SPF and GF mice (Figures 22A & 22B). In the spleen, on day 3, both $CD45^-$ and $CD45^+$ CECs from SPF mice expressed significantly higher levels of arginase-1 relative to $CD45^-$ and $CD45^+$ CECs from GF mice ($p<0.01$) (Figure 22C). This same pattern was observed on day 6 in the spleen ($p<0.001$) (Figure 22C).

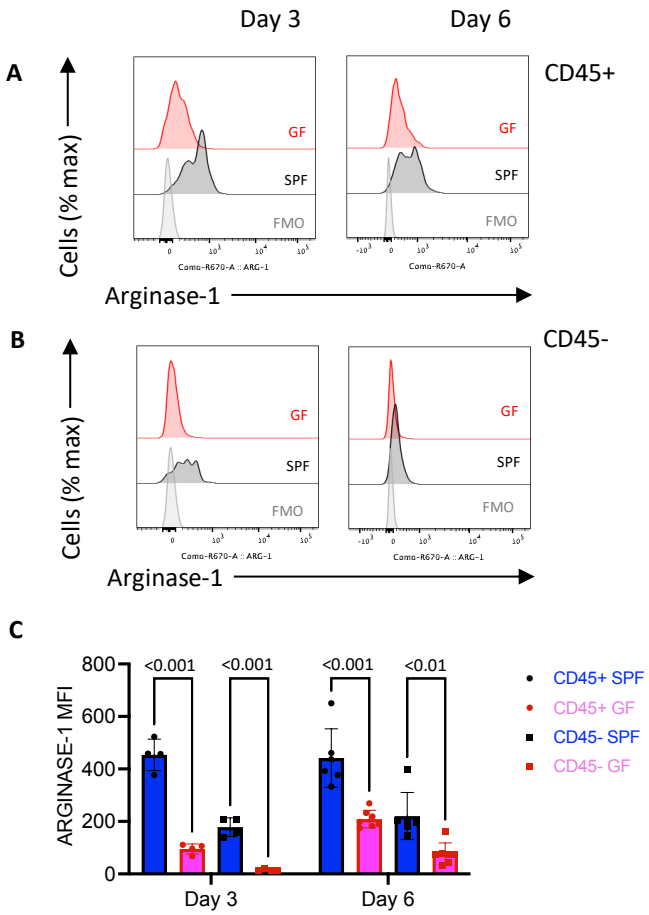

Figure 21: CD45$^+$ and CD45$^-$ CECs from the guts of SPF mice expressed significantly higher levels of arginase-1 compared to CD45$^+$ and CD45$^-$ CECs from the guts of GF mice on days 3 and 6.

Cells were prepared as in Figures 4 and 5. (A) Representative MFI plots for gut CD45$^+$ CECs from SPF and GF mice. Each sample was plotted against the negative control for arginase-1, the FMO. (B) Representative MFI plots for CD45$^-$ CECs from the guts of SPF and GF mice. Each sample was plotted against the negative control for Arginase-1, the FMO. (C) At all time points, CD45$^+$ CECs from the guts of SPF mice expressed significantly higher levels of arginase-1 compared to CD45$^+$ CECs from the GF gut ($p<0.001$). (C) At all time points, CD45$^-$ CECs from the guts of SPF mice expressed significantly higher levels of arginase-1 compared to CD45$^-$ CECs from the GF gut ($p<0.01$). Samples were not collected at the day 1 time point due to the lack of sufficient cell count in the tissues needed for intracellular staining. Results were analyzed with mixed effects model followed by Tukey's multiple comparisons test (n= 4 D3 SPF Gut, n= 4 D3 GF Gut, n= 6 D6 SPF Gut, n= 6 D6 GF Gut. Shown are mean ± SEM). Data is presented from single experiments which have been repeated once. Sex of mice was not reported since it was not determined at euthanasia.

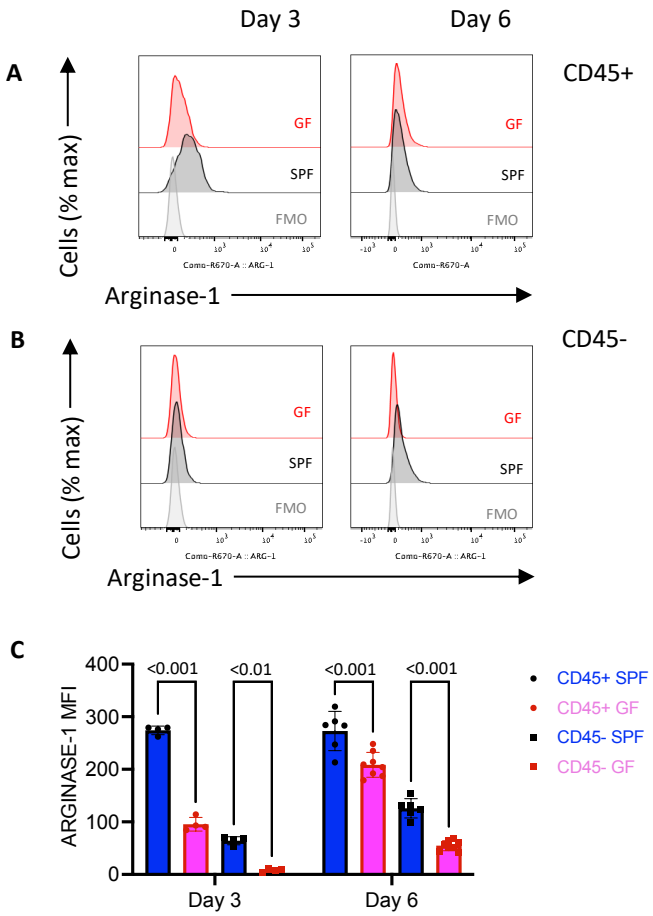

Figure 22: CD45$^+$ and CD45$^-$ CECs from spleens of SPF mice expressed significantly higher levels of arginase-1 compared to CD45$^+$ and CD45$^-$ CECs from the spleens of GF mice on days 3 and 6.

Cells were prepared as in Figures 4 and 5. (A) Representative MFI plots for CD45$^+$ CECs from the spleens of SPF and GF mice. Each sample was plotted against the negative control for arginase-1, the FMO. (B) Representative MFI plots for CD45$^-$ CECs from the spleens of SPF and GF mice. Each sample was plotted against the negative control for arginase-1, the FMO. (C) At all time points, CD45$^+$ CECs from the spleens of SPF mice expressed significantly higher levels of arginase-1 compared to CD45$^+$ CECs from the spleens of GF mice ($p < 0.0001$ for all comparisons). (C) At all time points, CD45$^-$ CECs from the spleens of SPF mice expressed significantly higher levels of arginase-1 compared to CD45$^-$ CECs from the spleens of GF mice ($p = 0.0015$, $p < 0.0001$, day 3, day 6, respectively). Results were analyzed with mixed effects model followed by Tukey's multiple comparisons test (n= 4 D3 SPF Spleen, n= 4 D3 GF Spleen, n= 8 D6 SPF Spleen, n= 8 D6 GF Spleen. Shown are mean ± SEM). Sex of mice was not reported since it was not determined at euthanasia.

3.4 AIM 1C

$CD45^+$ CECs in both the gut and spleen have higher expression of all measured TLRs compared to $CD45^-$ CECs

To further investigate the observed functional differences of CECs in SPF and GF mice I chose to examine the expression of various TLRs. Toll-like receptor 1 (TLR1) expression was measured on the surface of $CD45^-$ and $CD45^+$ CECs in the gut and spleen of SPF mice (Figure 23B). An FMO for TLR1 was used to set the positive gate (Figure 20A). In both the gut and the spleen, significantly higher percentages of $CD45^+$ CECs expressed TLR1 relative to $CD45^-$ CECs ($p<0.001$) (Figure 23C). MFI was used to measure the relative amount of TLR1 on the surface of CECs in the gut and the spleen (Figure 23D). An FMO was used as a negative control for TLR1 MFI (Figure 23D). Once again, in the spleen and gut, $CD45^+$ CECs expressed significantly higher levels of TLR1 relative to $CD45^-$ CECs ($p<0.001$) (Figure 23E). Essentially, almost 0% of $CD45^-$ CECs express TLR1 on their surface, whereas 30% of $CD45^+$ CECs in the gut and 40% in the spleen express TLR1 (Figure 23).

Next, toll-like receptor 4 (TLR4) expression on $CD45^-$ and $CD45^+$ CECs from the gut and spleen of SPF mice was investigated (Figure 24B). An FMO for TLR4 was used to set the positive gate (Figure 24A). In both the gut and the spleen, significantly higher percentages of $CD45^+$ CECs expressed TLR4 relative to $CD45^-$ CECs ($p<0.001$) (Figure 24C). MFI was used to measure the relative amount of TLR4 on the surface of CECs in the gut and the spleen (Figure 24D). An FMO was used as a negative control for TLR4 MFI (Figure 24D). Once again, in the spleen and gut, $CD45^+$ CECs expressed significantly higher levels of TLR4 relative to $CD45^-$ CECs ($p<0.001$) (Figure

24E). When comparing TLR4 expression, $CD45^-$ CECs had almost no TLR4 expression, whereas about 10% of $CD45^+$ CECs in the spleen and gut expressed TLR4 (Figure 24).

Lastly, toll-like receptor 9 (TLR9) expression was measured in the cytosol of $CD45^-$ and $CD45^+$ CECs from the gut and spleen of SPF mice (Figure 25A). MFI was used to measure the relative amount of TLR9 in the cytosol of CECs from the gut and the spleen. An FMO was used as a negative control for TLR9 MFI (Figure 25A). In both the gut and the spleen, significantly higher percentages of $CD45^+$ CECs expressed TLR9 relative to $CD45^-$ CECs ($p<0.001$) (Figure 25B). Intracellularly, $CD45^+$ CECs in both the spleen and gut expressed significantly higher levels of TLR9 relative to $CD45^-$ CECs (Figure 25).

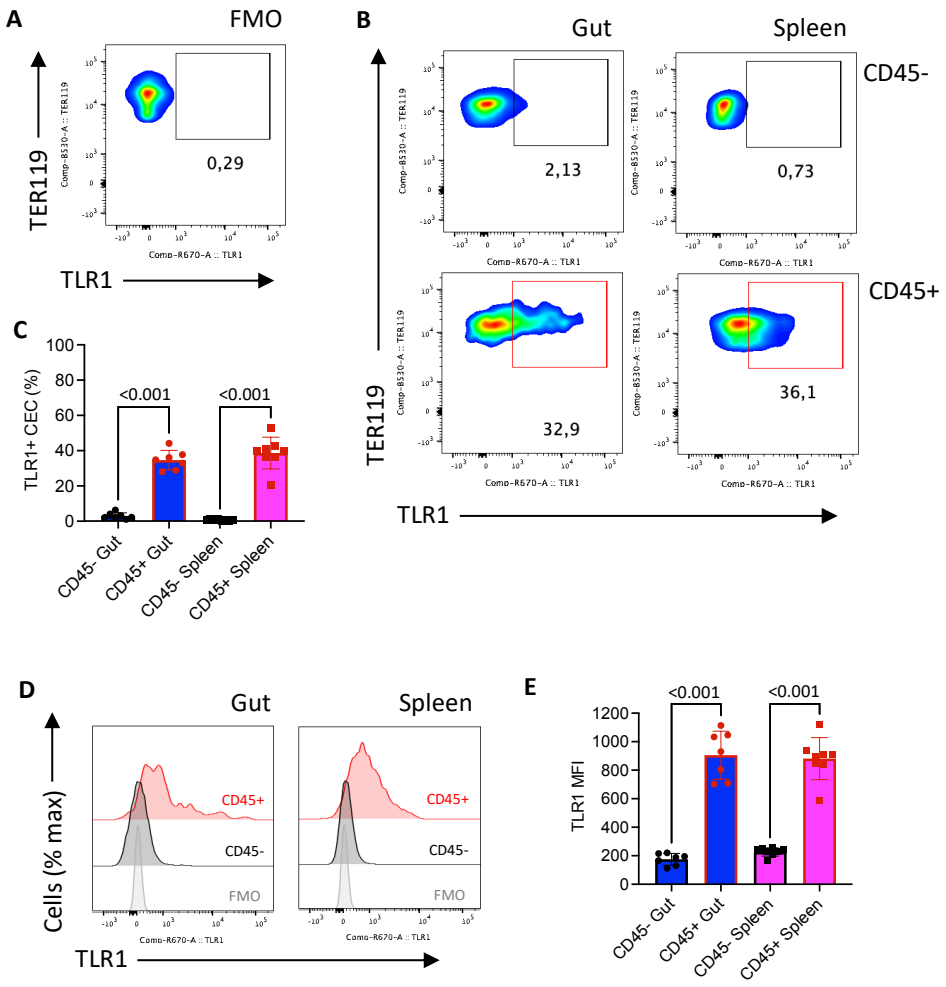

Figure 23: Greater percentages of CD45$^+$ CECs from the gut and spleen expressed TLR1, and at higher levels, compared to CD45$^-$ CECs.

Cells were prepared as in Figures 4 and 5. (A) Representative plot of negative control for TLR1 that was used to set the positive population gate. (B) Representative plots of TLR1$^+$ CD45$^-$ CECs and TLR1$^+$ CD45$^+$ CECs from the gut and spleen of SPF mice. (C) Significantly higher percentages of CD45+ CECs from both the gut and spleen expressed TLR1 compared to CD45$^-$ CECs from the gut and spleen ($p< 0.001$). (D) Representative MFI plots for CD45$^+$ and CD45$^-$ CECs from the gut and spleen of SPF mice. Each sample was plotted against the negative control for TLR1, the FMO. (D) CD45$^+$ CECs from both the gut and spleen expressed significantly higher levels of TLR1 compared to CD45$^-$ CECs from the gut and spleen ($p< 0.001$). Results were analyzed with Ordinary one-way ANOVA followed by Tukey's multiple comparisons test (n= 7 Gut, n= 8 Spleen. Shown are mean ± SEM). Data is presented from a single experiment. Sex of mice was not reported since it was not determined at euthanasia.

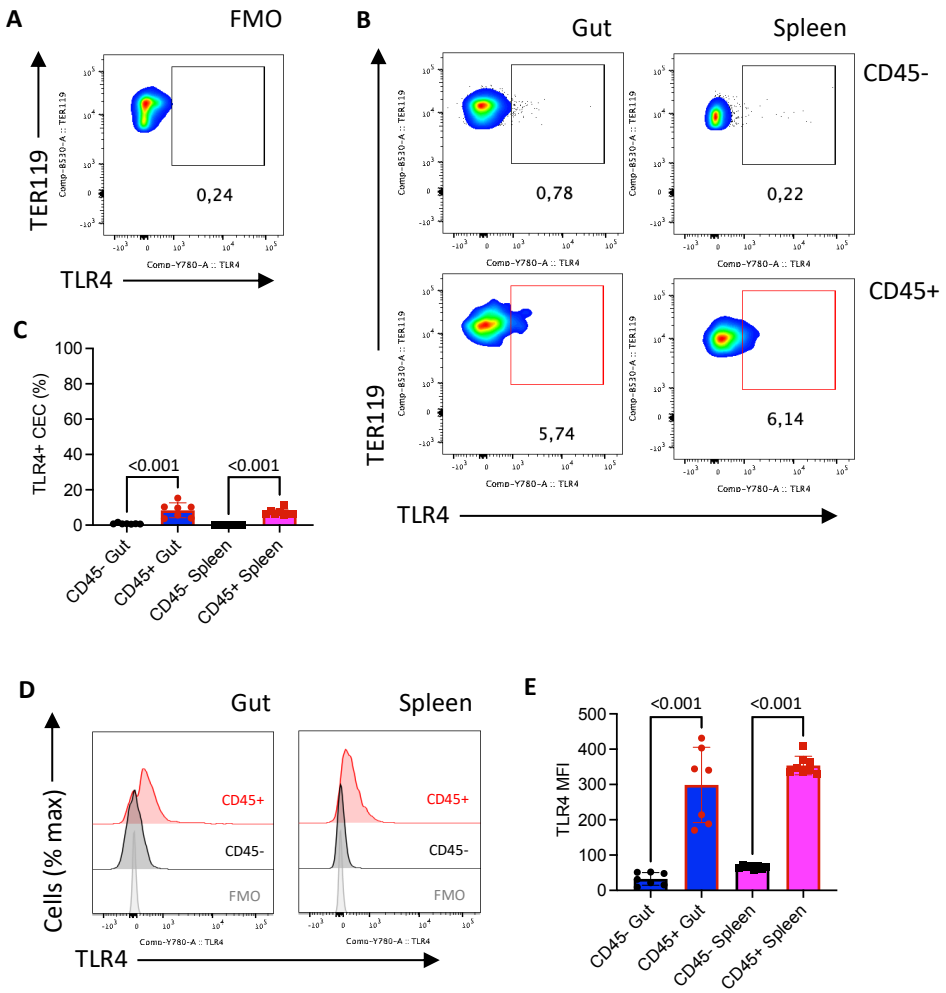

Figure 24: Greater percentages of CD45$^+$ CECs from the gut and spleen expressed TLR4, and at higher levels, compared to CD45$^-$ CECs.

Cells were prepared as in Figures 4 and 5. (A) Representative plot of negative control for TLR4 that was used to set the positive population gate. (B) Representative plots of TLR4$^+$ CD45$^-$ CECs and TLR4$^+$ CD45$^+$ CECs from the gut and spleen of SPF mice. (C) Significantly higher percentages of CD45$^+$ CECs from both the gut and spleen expressed TLR4 compared to CD45$^-$ CECs from the gut and spleen ($p<0.001$). (D) Representative MFI plots for CD45$^+$ and CD45$^-$ CECs from the gut and spleen of SPF mice. Each sample was plotted against the negative control for TLR4, the FMO. (D) CD45$^+$ CECs in both the gut and spleen expressed significantly higher levels of TLR4 compared to CD45$^-$ CECs from the gut and spleen ($p<0.001$). Results were analyzed with Ordinary one-way ANOVA followed by Tukey's multiple comparisons test (n= 7 Gut, n= 8 Spleen. Shown are mean ± SEM). Data is presented from a single experiment. Sex of mice was not reported since it was not determined at euthanasia.

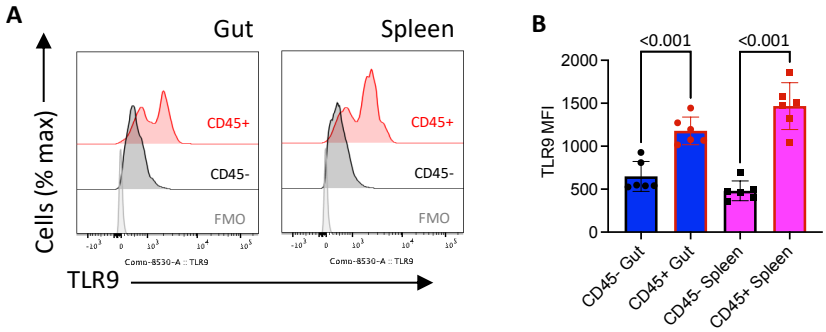

Figure 25: CD45$^+$ CECs in both the gut and spleen express significantly higher levels of toll-like receptor 9 (TLR9) compared to CD45$^-$ CECs.

Cells were prepared as in Figures 4 and 5. (A) Representative MFI plots for CD45$^+$ and CD45$^-$ CECs from the gut and spleen of SPF mice. Each sample was plotted against the negative control for TLR9, the FMO. (B) CD45$^+$ CECs from both the gut and the spleen expressed significantly higher levels of TLR9 intracellularly compared to CD45$^-$ CECs from the gut and spleen ($p<0.001$). Results were analyzed with Ordinary one-way ANOVA followed by Tukey's multiple comparisons test (n= 6 Gut, n= 6 Spleen. Shown are mean ± SEM). Data is presented from a single experiment. Sex of mice was not reported since it was not determined at euthanasia.

3.5 AIM 2

Long-term CD71 depletions

The functional characterization of CECs in SPF and GF mice showed that the CEC phenotype changed in the absence of the microbiome. To further support the interaction between CECs and the microbiome I found that $CD45^+$ CECs, specifically, expressed TLRs. Therefore, I chose to investigate whether a single depletion of CD71 expressing cells would have any lasting effects on the small intestine microbiome. CECs were depleted on day 3 from a single litter. The litter was randomly split into the control and treated groups, and CECs were depleted in the treated group. The litter was then left until day 22. This time point was selected since it is when pups are weaned from their mothers. Around this time, they have begun eating solid food, and their microbiome is diversified (85). The first analysis metric used was alpha diversity or within-sample diversity. No differences were detected in alpha diversity including Shannon's Diversity, Faith's phylogenetic diversity and observed operational taxonomic units (OTUs) (Figure 26A-C). Next, beta diversity or between-sample diversity was analyzed using both weighted and unweighted UniFrac (Figures 26D & 26F). Analysis of the unweighted UniFrac PCoA showed that there were no differences in the composition of the microbial populations based on the absence or presence of taxonomic groups (Figure 26E). Moreover, analysis of the weighted UniFrac PCoA showed that there were no differences in the composition of the bacterial populations in the control and treated mice based on the abundance of taxonomic groups (Figure 26G). Finally, on day 22, there were no differences in bacterial composition at all taxonomic levels. The mean relative abundance was recorded at the phylum level (Figure 26H).

The taxonomic bar plots that were used to calculate mean relative abundance are included (Figure 28A).

The next selected time point for the microbial analysis was day 36. This is two weeks post-weaning when the mice have been consuming a normal solid food diet. This time point was selected to allow for the settling of the microbiome. It is during this time that there is a diversification of the microbiome. No differences were detected in alpha diversity including Shannon's Diversity, Faith's phylogenetic diversity and observed operational taxonomic units (OTUs) (Figure 27A-C). Following, beta diversity was analyzed using both weighted and unweighted UniFrac (Figures 27D & 27F). Analysis of the unweighted UniFrac PCoA showed that there were no differences (Figure 27E). However, analysis of the weighted UniFrac PCoA showed differences in the composition of the control and treated groups ($p<0.05$)(Figure 27G). On day 36, there were no differences in bacterial composition at any taxonomic level. The mean relative abundance was visualized at the phylum level due to the diversity of the microbial population (Figure 27H). The taxonomic bar plots that were used to calculate mean relative abundance are included (Figure 28B).

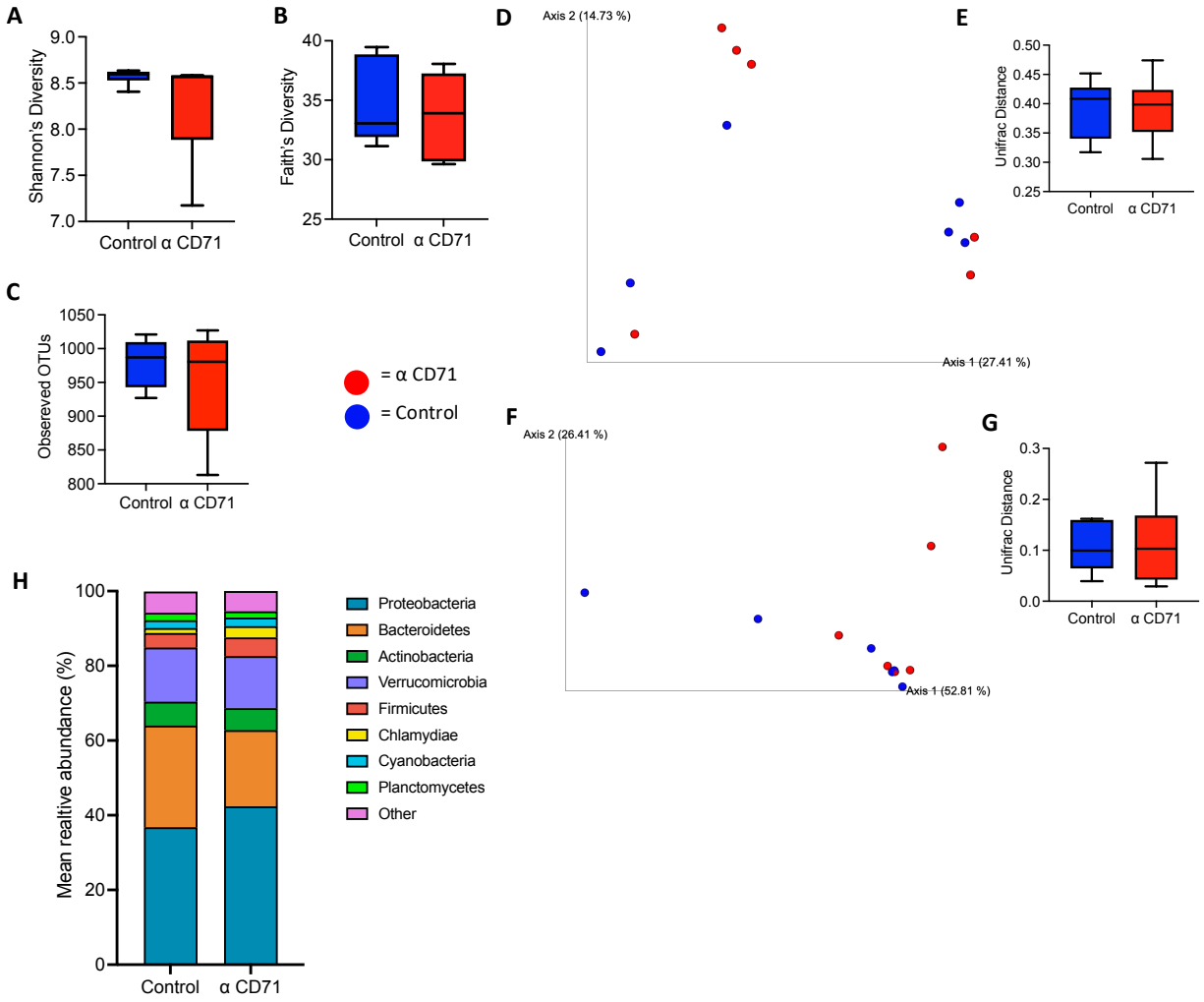

Figure 26: There were no differences in microbial diversity in the small intestine on day 22 when CECs were depleted on day 3.

Litter mates were randomly injected with either control antibody or anti-CD71 antibody on day 3. All mice were selected from the same litter to eliminate cage effects. On day 22, mice were euthanized and stool from the small intestine was collected for isolation of microbial DNA. Isolated DNA was submitted for 16S rRNA sequencing, and QIIME2 was used to analyze raw sequences. Within sample diversity was analyzed by the following tests: Shannon's diversity (A), Faith's diversity (B), and observed Operational Taxonomic Units (OTUs) (C). Between-sample diversity was analyzed by the following tests: unweighted UniFrac (D), and weighted UniFrac (F). PERMANOVA was used to analyze beta diversity unweighted UniFrac (E) and weighted UniFrac (G). (H) Mean relative abundance at phylum level taxonomic classification. Control mice n=6 3f 3m; treated mice n=6 5f 1m. Data is presented from a single experiment.

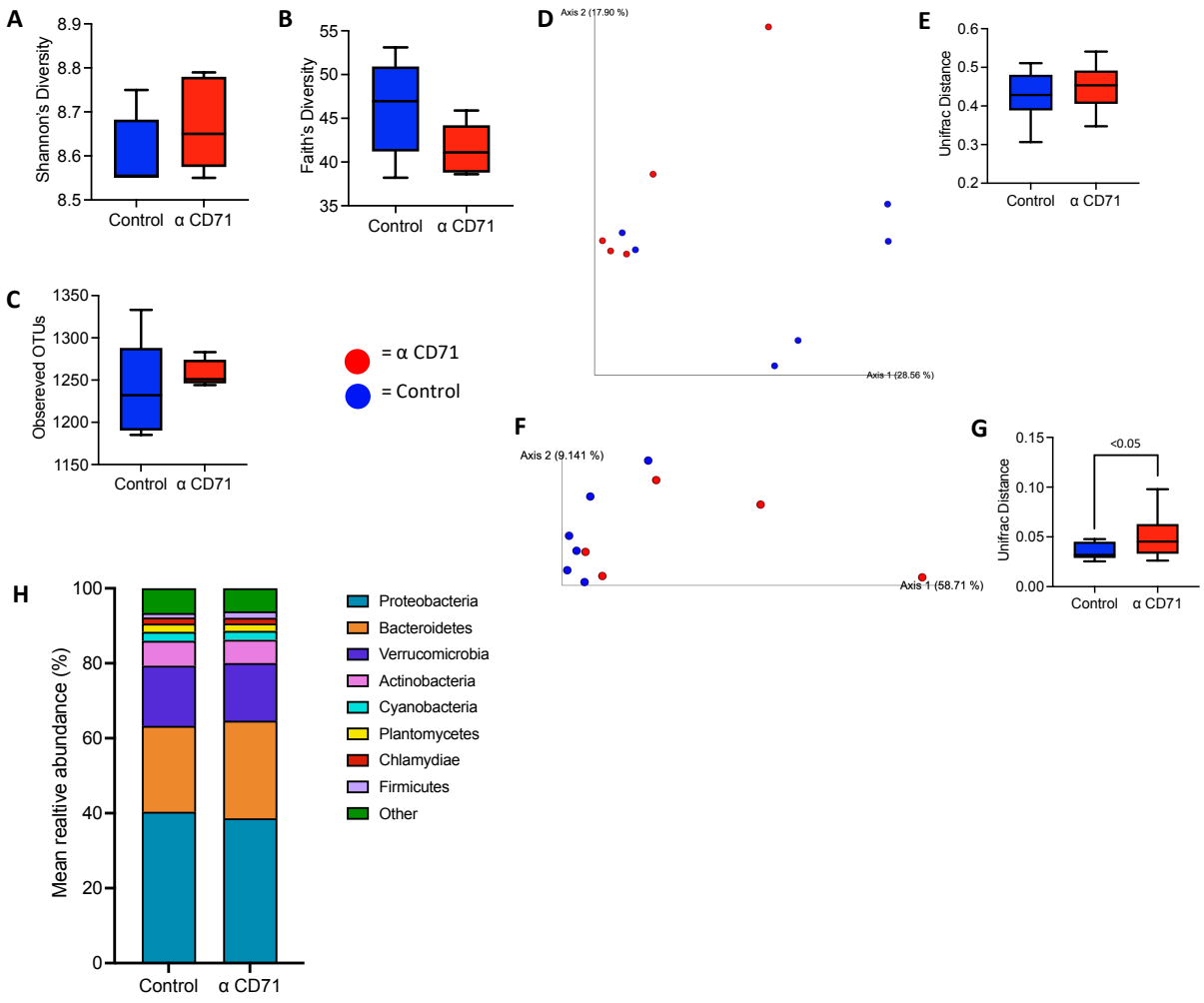

Figure 27: There were no differences in microbial diversity in the small intestine on day 36 when CECs were depleted on day 3.

Litter mates were randomly injected with either control antibody or anti-CD71 antibody on day 3. All mice were selected from the same litter to eliminate cage effects. On day 36, mice were euthanized and stool from the small intestine was collected for isolation of microbial DNA. Isolated DNA was submitted for 16S rRNA sequencing, and QIIME2 was used to analyze raw sequences. Within sample diversity was analyzed by the following tests: Shannon's diversity (A), Faith's diversity (B), and observed Operational Taxonomic Units (OTUs) (C). Between-sample diversity was analyzed by the following tests: unweighted UniFrac (D), and weighted UniFrac (F). PERMANOVA was used to analyze beta diversity between unweighted Unifrac (E) and weighted Unifrac (G) ($p<0.05$). (H) Mean relative abundance at phylum level taxonomic classification. Control mice n=6, 4f 2m; treated mice n=5, 3f 2m. Data is presented from a single experiment.

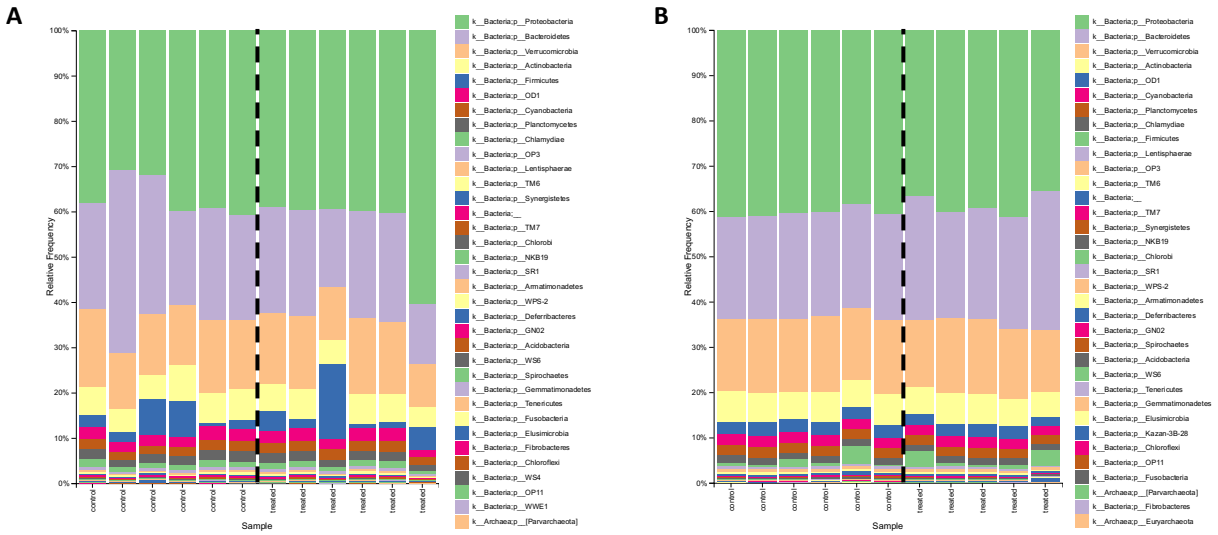

Figure 28: Overview Taxonomic Bar Plots of Day 22 and Day 36 groups.

Samples were obtained and processed as described in Figures 26 and 27. (A) The taxonomic bar plot for day 22 samples at the Phylum level. (B) The taxonomic bar plot for Day 36 samples at the Phylum level.

4. Discussion

The proper establishment of the microbiome in the GI tract of newborns is essential for overall health. Studies have shown that dysregulation of the early microbiome may predispose newborns to autoimmune disorders later in life (86,87). Therefore, it is crucial that the immune system can tolerate the colonization of commensal microbes. Immune tolerance is promoted in the GI tract through the release of anti-inflammatory cytokines such as TGF-β, IL-10 and IL-27 (88). These cytokines promote the differentiation and proliferation of $FOXP3^+$ Treg cells, discouraging unwarranted immune activation (89). Correspondingly, CECs in newborns have a suppressive role within the immune system (58). Past studies have been predominantly carried out using splenic CECs, thus, the functionality of CECs in the GI tract remains a novel area of research. The role of CECs in the establishment of the microbiome is an area where there is much more to be discovered.

4.1 CEC functionality in newborn wild-type mice

My first objective was to characterize the functionality of $CD45^-$ and $CD45^+$ CECs in newborns. I chose to investigate the spleen since it is a secondary lymphoid organ and a major site for EE (90). Additionally, previous studies have shown that CECs are enriched in the spleen. The small intestine and colon were investigated collectively as the gut, to explore the influence of the body site, as well as the gut microbiota. Three-time points were chosen for comparisons: day 1, day 3, and day 6. These time points were chosen to compare functionality as the early microbiome settled post-birth.

I first examined the expression of CECs in both tissues. In the gut, the frequency of CECs was relatively constant through all periods, remaining at approximately 20% (Figure 6). In contrast, in the spleen, I observed that on days 3 and 6 there were significant increases in the percentages of CECs relative to day 1 (Figure 6). This increase is due to the rapid development that the pups experience. Thus, a swift expansion of erythrocytes is required as the pups grow and develop (51). To produce adequate levels of erythrocytes the spleen undergoes EE (84). This would explain why on day 1 there are approximately 20% CECs, whereas on days 3 and 6 it rises to roughly 45% (Figure 6).

Since CD45 is expressed on hematopoietic cells and is involved in immune function, I explored the differences between $CD45^-$ and $CD45^+$ CECs in both the spleen and the gut of newborns. I had hypothesized that $CD45^+$ CECs would be more potent immune mediators, and this would be manifested through a higher expression of the measured markers. Correspondingly, in both the spleen and the gut, I found that $CD45^+$ CECs expressed higher frequencies of all measured immune mediators relative to $CD45^-$ CECs (Figures 7-11). I measured the expression of VISTA, ROS, TGF-β and arginase-1. This pattern was observed during all recorded time points in the spleen and gut of newborns. Correspondingly, it has been shown that $CD45^+$ CECs in the adult spleen express higher levels of ROS, VISTA, and arginase-1 (56). Interestingly, Hermiston and colleagues showed that CD45 functions as a modulator for cell signalling responses to external stimuli (59). Similarly, numerous studies of $CD45^-$ mice and humans found that they were prone to developing severe-combined immunodeficiency (SCID) (91) (92) (93). These previous findings highlight the importance of CD45 signalling in immune function.

I next wanted to compare the functionality of $CD45^+$ and $CD45^-$ CECs in the spleen relative to the gut. I hypothesized that $CD45^+$ and $CD45^-$ CECs in the gut would have differential expression of VISTA, ROS, TGF-β and Arginase-1 relative to that $CD45^+$ and $CD45^-$ CECs in the spleen. Interestingly, regarding VISTA, there were no differences in the expression of $CD45^+$ CECs in the spleen and gut on day 1 (Figure 7). However, by days 3 and 6, a significantly greater percentage of $CD45^+$ CECs in the gut expressed VISTA relative to the spleen (Figure 7). Additionally, $CD45^+$ CECs in the gut also expressed VISTA at significantly higher levels relative to the spleen (Figure 8). This was also observed with regards to TGF-β and Arginase-1 expression by $CD45^+$ CECs in the gut and the spleen (Figures 9 & 10). These findings indicate that $CD45^+$ CECs differ phenotypically, depending on the body site. CECs are generated in the spleen, a secondary lymphoid organ, and then travel to the GI tract. Therefore, the functional variation observed in CECs between the spleen and the gut may indicate the influence of surrounding environments. Furthermore, it is important to recognize the distinctive patterns observed during the various time points. On day 1, it is expected that most observed effects are due to influences from the mother and embryonic development. The microbiome has not drastically impacted the immune system in the first 24 hours of life. However, by days 3 and 6, the establishment of the early microbiome would begin to influence the surrounding environment and immune system.

My study established that $CD45^-$ CECs expressed significantly lower levels of the measured immune factors; nonetheless, I wanted to explore whether there were similar patterns observed across both tissues as observed with $CD45^+$ CECs. Interestingly, the functional

variations of $CD45^-$ CECs in the two tissues were not as significant as the patterns observed in $CD45^+$ CECs.

I decided to examine whether CECs expressed TLRs to rationalize the functional differences I observed. Comparably, I found that $CD45^+$ CECs expressed significantly higher levels of various TLRs in comparison to $CD45^-$ CECs (Figures 23-25). The presence of TLRs on CECs may point to their capability of sensing and reacting to the surrounding environment. Essentially, I found that $CD45^+$ CECs were more immune potent and expressed higher levels of TLRs compared to mature $CD45^-$ CECs.

4.2 CEC functionality in the GF mouse model

Once I had characterized the functional differences of $CD45^-$ and $CD45^+$ CECs in SPF mice, my next objective was to characterize any functional differences between CECs in SPF and GF mice. I observed that GF mice had significantly reduced frequencies of CECs in both the spleen and the gut on day 1 (Figure 12). However, these differences were resolved by days 3 and 6, when both GF and SPF mice expressed similar frequencies of CECs in the spleen and the gut.

Relatedly, it has been found that pregnant GF mice experienced altered metabolic functions due to the lack of the microbiome (94). Additionally, other studies have found that pregnant GF mice experienced altered immune functions, suggesting that the microbiome plays a modulatory role during pregnancy (95). Similarly, Dunsmore et al (2019) found that pregnant mothers with IBD experienced altered frequency and functionality of CECs (57). Moreover,

studies have shown that IBD is associated with microbial dysbiosis (96–98). Therefore, it is possible that the lack of the microbiome in the pregnant GF mice resulted in a lowered frequency of CECs. This could explain the reduced frequency of CECs that was observed during day 1 in GF mice since early immunity in newborns heavily relies on the mother (99). However, further studies need to be completed to determine whether this is the case. A study to determine this could be to characterize CECs from the pregnant GF mother. Lastly, although measurements were not recorded, it should be noted that there were no overt differences between the SPF and GF mice. Similarly, no overt differences were observed in both spleen and gut between the groups.

I next hypothesized that CECs would have functional differences in GF mice due to the lack of a microbiome. On day 1, I observed no differences in the percentage of CECs expressing VISTA on their cell surface in either organ. However, percentage differences emerged by day 3 in the spleen and gut (Figures 13-14). Moreover, it was observed that on days 3 and 6, $CD45^+$ CECs in the spleen and gut of SPF mice expressed higher levels of Arginase-1 (Figures 21-22). Interestingly, Elahi et al (2013) showed that arginase activity was essential for the immune suppressive abilities of CECs (53). Thus, the decreased levels of Arginase-1 in GF CECs may indicate a reduction in immune-suppressive properties. Furthermore, in the gut on both days 3 and 6, I found that $CD45^+$ CECs from SPF mice expressed higher levels of TGF-β (Figure 19). TGF-β plays a crucial role in promoting tolerance to the resident microorganisms; therefore, the lack of microbiome in GF mice can explain the observed decrease in expression. I believe it would be useful to investigate PRR expression on CECs in GF mice since other immune cells in GF mice

express lower levels of TLRs (47). This could help further explain the functional differences of $CD45^+$ CECs dependent on the microbiome. A possible study to further investigate the functional differences of $CD45^+$ CECs in SPF and GF mice could be to measure their suppressive capabilities *in vitro*. This would provide further information on any functional differences observed in the two populations.

I next sought to compare the functionality of $CD45^-$ CECs in SPF and GF mice. On day 6, significantly higher percentages of $CD45^-$ CECs in the spleen and gut of SPF mice expressed VISTA (Figures 15-16). Similarly, on days 3 and 6, $CD45^-$ CECs in the spleen and gut expressed higher levels of VISTA (MFI measurements) (Figure 17-18). In contrast, on day 1, I observed that CD45- CECs in the gut of GF mice expressed higher levels of VISTA relative to SPF mice (Figure 15). Moreover, it was observed that on days 3 and 6, CD45- CECs in the spleen and gut of SPF mice expressed higher levels of Arginase-1 (Figures 21-22). Interestingly, there were no differences observed in TGF- β expression. These findings indicate that CD45- CECs, although less immune-suppressive, differ functionally in the GF mouse model.

I had established that $CD45^+$ CECs expressed various TLRs, whereas $CD45^-$ CECs expressed minimal levels (Figures 23-25). Therefore, the variation in the functionality of $CD45^-$ CECs in SPF and GF mice is likely not due to microbial sensing abilities but rather intrinsic differences caused by the lack of a microbiome. This same phenomenon may also explain the differences observed in the spleen of SPF and GF mice. As a secondary lymphoid organ, the spleen is responsible for the generation of leukocytes. Cells generated in the spleen have not yet been exposed to the

factors that are present throughout the GI tract. Therefore, it is crucial to further investigate the functionality of CECs to understand the basis of the observed variations. Towards this end, single-cell RNA sequencing on the populations of $CD45^-$ and $CD45^+$ CECs from the spleen and gut of SPF and GF mice may be informative.

4.3 Long-term depletions

I established that there were functional differences between CECs in SPF and GF mice. Additionally, previous data collected from our lab showed that the depletion of CD71 expressing cells on day 3 results in microbial dysbiosis in the small intestine on day 4 (unpublished), indicating that a short-term depletion of CD71 expressing cells leads to significant changes in the microbial population in the small intestine. Based on this information, I planned to investigate whether a single depletion of CD71 cells in postnatal mice had any lasting effects on the small intestine microbiome. The pups were treated on day 3, as per the previous studies. The first litter of pups was left until weaning, day 22. The second litter of pups was left until day 36, two weeks post-weaning. This time point was selected to allow the microbiome to further diversify due to the pups consuming the normal chow diet. Hung and colleagues found that six-week-old mice experienced a significant increase in the diversity of their microbiome relative to the neonatal period (100). This is due to the transition from milk to a solid food diet. In humans, this diversification of the microbiome is observed at approximately four months old and continues until three years of age, when a mature microbiome has been established (101).

I found that there were no long-lasting effects of CD71 cell depletion on the small intestine microbiome on day 22 (Figure 26). The control and treatment groups had no differences in alpha and beta diversity (Figure 26). Interestingly, on day 36 there was a variation between the control and treated bacterial populations when looking at the weighted UniFrac ($p<0.05$) (Figure 27).

Having not accounted for sex at the time of depletion may have contributed to the variability within the treatment groups. Sex is a key driver of microbiome composition, accordingly, several studies have illustrated the sex-related differences in the gut microbiome (24,25,102). Therefore, this is a significant limitation of the present study and dictates caution in the interpretation of the data and in drawing any conclusions from the results. Overall, the variance in the results, in part from sex, may be the reason for the lack of significance in the data. Moreover, because both control and treated mice were housed together post CD71 depletion the effects of cohabitation cannot be ruled out. Several studies have shown that cohabitation influences the gut microbiota of individuals (103–105). Specifically, Finnicum et al. found that cohabitation between twins resulted in similar alpha diversity and decreased Bray-Curtis distances relative to twins that were non-cohabitating (103).

4.4 Limitations

A limitation I faced when conducting the SPF and GF comparisons was the timing of the pregnancies. It was not possible to match the births so that SPF and GF mice of the same age could be processed at once. To minimize the effects of this, all flow cytometry experiments

were acquired with the same settings. Another drawback I faced was collecting adequate levels of cells from the guts of the neonatal mice. Due to the nature of gut cell isolation and the small size of the tissue, it was difficult to collect enough cells to run multiple panels and their required controls. This limited my ability to create various panels to test a large variety of markers. Thus, I needed to select key markers of interest or conduct additional experiments for different panels of markers.

While conducting the long-term CD71 cell depletions, I was faced with additional challenges. The first limitation I faced was the generation of adequate litter sizes. In these studies, all control and treated mice were from the same litter. The C5BL/6 breeding pairs were generating small litters and the pups were frequently cannibalized by the mother when stressed. Therefore, these depletions were done on BALB/c mice. Using a single litter per experiment prevents any cage effects, such as variation of the microbiome between cages and litters. Additionally, it was not possible to ensure that the single administration of the CD71 antibody was successful. When doing a short-term depletion, normally the spleen is processed and analyzed using flow cytometry to characterize the frequency of CECs. However, since the mice were maintained for a minimum of three weeks post-depletion this was not possible. The final limitation I faced during these experiments was inability to account for sex at the time of depletion. Since on day 3, the sex of the pups was not visibly apparent to me, the sex of the pups was not taken into account. This is a limitation because past research has clearly shown that sex impacts the microbiome, however, in these experiments, it was not accounted for at the time of depletion.

4.5 Future directions and Significance

Effectively, the establishment of a balanced microbiome is fundamental for the overall health of the newborn. The process of microbial colonization in the Gi tract involves the interaction of hosts and microbes as well as other external factors and influences (83,106,107). However, in some cases, the microbiome is disrupted, and this dysbiosis can negatively impact the infant in various ways (108). Therefore, I studied the relationship between CECs and the microbiome to explore possible interactions. I found that $CD45^+$ CECs in the newborn gut and spleen are much more immune potent compared to their $CD45^-$ counterparts. Moreover, the results showed that CECs are a heterogeneous population of cells that vary phenotypically depending on the body site. Additionally, the phenotype of these CECs was altered in the GF model likely due to microbial sensing and independent mechanisms. Past data has shown that CEC frequency and functionality were altered in pregnant women with IBD (57). Accordingly, studies have shown that individuals with IBD experienced altered microbial composition (96,109). Essentially, pointing to an association between the functionality and frequency of CECs and the microbiome. As mentioned, it would be worthwhile to investigate the functional differences of $CD45^+$ CECs from SPF and GF mice *in vitro*. These results could provide a deeper understanding of the possible functional differences between CECs in the two groups. It would also be important to study the CEC populations in pregnant SPF and GF mice to address the role of the mother on the developing fetus. Furthermore, I investigated the effects of long-term CEC depletions on the small intestinal microbiome. My findings indicated that transient depletion of CECs was not sufficient to cause long-term microbial dysbiosis by day 22 or day 36. However, it would be valuable to repeat this study to address the possible influence of cohabitation.

Ultimately, this study has generated novel data suggesting communication between the microbiome and CECs. It is crucial to further investigate these findings to provide us with a deeper understanding of CECs and their role in the proper establishment of the early microbiome. These results were obtained in combination with ongoing research and may potentially identify a novel and critical role for CECs in immune tolerance and microbial dysbiosis.

References

1. Valdes AM, Walter J, Segal E, Spector TD. Role of the gut microbiota in nutrition and health. BMJ. 2018 Jun 13;k2179.

2. Jandhyala SM. Role of the normal gut microbiota. WJG. 2015;21(29):8787.

3. Delungahawatta T, Amin JY, Stanisz AM, Bienenstock J, Forsythe P, Kunze WA. Antibiotic Driven Changes in Gut Motility Suggest Direct Modulation of Enteric Nervous System. Front Neurosci. 2017 Oct 20;11:588.

4. Round JL, Mazmanian SK. The gut microbiota shapes intestinal immune responses during health and disease. Nat Rev Immunol. 2009 May;9(5):313–23.

5. De Vadder F, Grasset E, Mannerås Holm L, Karsenty G, Macpherson AJ, Olofsson LE, et al. Gut microbiota regulates maturation of the adult enteric nervous system via enteric serotonin networks. Proc Natl Acad Sci USA. 2018 Jun 19;115(25):6458–63.

6. Dekaboruah E, Suryavanshi MV, Chettri D, Verma AK. Human microbiome: an academic update on human body site specific surveillance and its possible role. Arch Microbiol. 2020 Oct;202(8):2147–67.

7. Chung H, Kasper DL. Microbiota-stimulated immune mechanisms to maintain gut homeostasis. Current Opinion in Immunology. 2010 Aug;22(4):455–60.

8. Rooks MG, Garrett WS. Gut microbiota, metabolites and host immunity. Nat Rev Immunol. 2016 Jun;16(6):341–52.

9. Lawley TD, Walker AW. Intestinal colonization resistance. Immunology. 2013 Jan;138(1):1–11.

10. Khan I, Bai Y, Zha L, Ullah N, Ullah H, Shah SRH, et al. Mechanism of the Gut Microbiota Colonization Resistance and Enteric Pathogen Infection. Front Cell Infect Microbiol. 2021 Dec 23;11:716299.

11. Hall AB, Tolonen AC, Xavier RJ. Human genetic variation and the gut microbiome in disease. Nat Rev Genet. 2017 Nov;18(11):690–9.

12. Diamond G, Beckloff N, Weinberg A, Kisich K. The Roles of Antimicrobial Peptides in Innate Host Defense. CPD. 2009 Jul 1;15(21):2377–92.

13. Coelho GDP, Ayres LFA, Barreto DS, Henriques BD, Prado MRMC, Passos CMD. Acquisition of microbiota according to the type of birth: an integrative review. Rev Latino-Am Enfermagem. 2021;29:e3446.

14. Gabriel I, Olejek A, Stencel-Gabriel K, Wielgoś M. The influence of maternal vaginal flora on the intestinal colonization in newborns and 3-month-old infants. The Journal of Maternal-Fetal & Neonatal Medicine. 2018 Jun 3;31(11):1448–53.

15. Mueller NT, Bakacs E, Combellick J, Grigoryan Z, Dominguez-Bello MG. The infant microbiome development: mom matters. Trends in Molecular Medicine. 2015 Feb;21(2):109–17.

16. Neu J, Rushing J. Cesarean Versus Vaginal Delivery: Long-term Infant Outcomes and the Hygiene Hypothesis. Clinics in Perinatology. 2011 Jun;38(2):321–31.

17. Kim G, Bae J, Kim MJ, Kwon H, Park G, Kim SJ, et al. Delayed Establishment of Gut Microbiota in Infants Delivered by Cesarean Section. Front Microbiol. 2020 Sep 11;11:2099.

18. Björkstén B, Sepp E, Julge K, Voor T, Mikelsaar M. Allergy development and the intestinal microflora during the first year of life. Journal of Allergy and Clinical Immunology. 2001 Oct;108(4):516–20.

19. Dogra S, Sakwinska O, Soh SE, Ngom-Bru C, Brück WM, Berger B, et al. Dynamics of Infant Gut Microbiota Are Influenced by Delivery Mode and Gestational Duration and Are Associated with Subsequent Adiposity. de Vos WM, Dominguez Bello MG, editors. mBio. 2015 Feb 27;6(1):e02419-14.

20. O'Sullivan A, Farver M, Smilowitz JT. Article Commentary: The Influence of Early Infant-Feeding Practices on the Intestinal Microbiome and Body Composition in Infants. Nutr Metab Insights. 2015 Jan;8s1:NMI.S29530.

21. Marcobal A, Barboza M, Froehlich JW, Block DE, German JB, Lebrilla CB, et al. Consumption of Human Milk Oligosaccharides by Gut-Related Microbes. J Agric Food Chem. 2010 May 12;58(9):5334–40.

22. Markle JGM, Frank DN, Mortin-Toth S, Robertson CE, Feazel LM, Rolle-Kampczyk U, et al. Sex Differences in the Gut Microbiome Drive Hormone-Dependent Regulation of Autoimmunity. Science. 2013 Mar;339(6123):1084–8.

23. Yoon K, Kim N. Roles of Sex Hormones and Gender in the Gut Microbiota. J Neurogastroenterol Motil. 2021 Jul 30;27(3):314–25.

24. Kim YS, Unno T, Kim BY, Park MS. Sex Differences in Gut Microbiota. World J Mens Health. 2020;38(1):48.

25. Org E, Mehrabian M, Parks BW, Shipkova P, Liu X, Drake TA, et al. Sex differences and hormonal effects on gut microbiota composition in mice. Gut Microbes. 2016 Jul 3;7(4):313–22.

26. Jašarević E, Morrison KE, Bale TL. Sex differences in the gut microbiome–brain axis across the lifespan. Phil Trans R Soc B. 2016 Feb 19;371(1688):20150122.

27. Ober C, Loisel DA, Gilad Y. Sex-specific genetic architecture of human disease. Nat Rev Genet. 2008 Dec;9(12):911–22.

28. Sisk CL, Foster DL. The neural basis of puberty and adolescence. Nat Neurosci. 2004 Oct;7(10):1040–7.

29. Yurkovetskiy L, Burrows M, Khan AA, Graham L, Volchkov P, Becker L, et al. Gender Bias in Autoimmunity Is Influenced by Microbiota. Immunity. 2013 Aug;39(2):400–12.

30. Tanaka M, Nakayama J. Development of the gut microbiota in infancy and its impact on health in later life. Allergology International. 2017 Oct;66(4):515–22.

31. Cresci GAM, Izzo K. Gut Microbiome. In: Adult Short Bowel Syndrome [Internet]. Elsevier; 2019 [cited 2022 Aug 15]. p. 45–54. Available from: https://linkinghub.elsevier.com/retrieve/pii/B9780128143308000044

32. Thompson MR, Kaminski JJ, Kurt-Jones EA, Fitzgerald KA. Pattern Recognition Receptors and the Innate Immune Response to Viral Infection. Viruses. 2011 Jun 23;3(6):920–40.

33. Kawai T, Akira S. The role of pattern-recognition receptors in innate immunity: update on Toll-like receptors. Nat Immunol. 2010 May;11(5):373–84.

34. Hato T, Dagher PC. How the Innate Immune System Senses Trouble and Causes Trouble. CJASN. 2015 Aug 7;10(8):1459–69.

35. Janeway CA. Approaching the Asymptote? Evolution and Revolution in Immunology. Cold Spring Harbor Symposia on Quantitative Biology. 1989 Jan 1;54(0):1–13.

36. Mackie S, Quinn M, Emery P. Rheumatoid Arthritis. In: The Autoimmune Diseases [Internet]. Elsevier; 2006 [cited 2022 Jun 12]. p. 417–36. Available from: https://linkinghub.elsevier.com/retrieve/pii/B9780125959612500354

37. Janeway CA. The immune system evolved to discriminate infectious nonself from noninfectious self. Immunology Today. 1992 Jan;13(1):11–6.

38. Medzhitov R. Toll-like receptors and innate immunity. Nat Rev Immunol. 2001 Nov;1(2):135–45.

39. Cornick S, Tawiah A, Chadee K. Roles and regulation of the mucus barrier in the gut. Tissue Barriers. 2015 Apr 3;3(1–2):e982426.

40. Herath M, Hosie S, Bornstein JC, Franks AE, Hill-Yardin EL. The Role of the Gastrointestinal Mucus System in Intestinal Homeostasis: Implications for Neurological Disorders. Front Cell Infect Microbiol. 2020 May 28;10:248.

41. Kong S, Zhang YH, Zhang W. Regulation of Intestinal Epithelial Cells Properties and Functions by Amino Acids. BioMed Research International. 2018;2018:1–10.

42. Min S, Kim S, Cho SW. Gastrointestinal tract modeling using organoids engineered with cellular and microbiota niches. Exp Mol Med. 2020 Feb;52(2):227–37.

43. Houghteling PD, Walker WA. Why Is Initial Bacterial Colonization of the Intestine Important to Infants' and Children's Health? Journal of Pediatric Gastroenterology & Nutrition. 2015 Mar;60(3):294–307.

44. Moore RE, Townsend SD. Temporal development of the infant gut microbiome. Open Biol. 2019 Sep;9(9):190128.

45. Nguyen TLA, Vieira-Silva S, Liston A, Raes J. How informative is the mouse for human gut microbiota research? Disease Models & Mechanisms. 2015 Jan 1;8(1):1–16.

46. Macpherson AJ, Harris NL. Interactions between commensal intestinal bacteria and the immune system. Nat Rev Immunol. 2004 Jun;4(6):478–85.

47. Akira S, Hemmi H. Recognition of pathogen-associated molecular patterns by TLR family. Immunology Letters. 2003 Jan;85(2):85–95.

48. Huhta H, Helminen O, Kauppila JH, Salo T, Porvari K, Saarnio J, et al. The Expression of Toll-like Receptors in Normal Human and Murine Gastrointestinal Organs and the Effect of Microbiome and Cancer. J Histochem Cytochem. 2016 Aug;64(8):470–82.

49. Hernández-Chirlaque C, Aranda CJ, Ocón B, Capitán-Cañadas F, Ortega-González M, Carrero JJ, et al. Germ-free and Antibiotic-treated Mice are Highly Susceptible to Epithelial Injury in DSS Colitis. ECCOJC. 2016 Nov;10(11):1324–35.

50. Chassaing B, Aitken JD, Malleshappa M, Vijay-Kumar M. Dextran Sulfate Sodium (DSS)-Induced Colitis in Mice. Current Protocols in Immunology [Internet]. 2014 Feb [cited 2022 Jun 24];104(1). Available from: https://onlinelibrary.wiley.com/doi/10.1002/0471142735.im1525s104

51. Elahi S, Mashhouri S. Immunological consequences of extramedullary erythropoiesis: immunoregulatory functions of CD71 $^{+}$ erythroid cells. Haematologica. 2020 Jun;105(6):1478–83.

52. Gomez-Lopez N, Romero R, Xu Y, Miller D, Unkel R, C. MacKenzie T, et al. Umbilical cord CD71+ erythroid cells are reduced in neonates born to women in spontaneous preterm labor. Am J Reprod Immunol. 2016 Oct;76(4):280–4.

53. Elahi S, Ertelt JM, Kinder JM, Jiang TT, Zhang X, Xin L, et al. Immunosuppressive CD71+ erythroid cells compromise neonatal host defence against infection. Nature. 2013 Dec 5;504(7478):158–62.

54. Kim C. Homeostatic and pathogenic extramedullary hematopoiesis. JBM. 2010 Mar;13.

55. Mebius RE, Kraal G. Structure and function of the spleen. Nat Rev Immunol. 2005 Aug;5(8):606–16.

56. Mashhouri S, Koleva P, Huynh M, Okoye I, Shahbaz S, Elahi S. Sex Matters: Physiological Abundance of Immuno-Regulatory CD71+ Erythroid Cells Impair Immunity in Females. Front Immunol. 2021 Jul 21;12:705197.

57. Dunsmore G, Koleva P, Ghobakhloo N, Sutton R, Ambrosio L, Meng X, et al. Lower Abundance and Impaired Function of CD71+ Erythroid Cells in Inflammatory Bowel Disease Patients During Pregnancy. Journal of Crohn's and Colitis. 2019 Feb 1;13(2):230–44.

58. Dunsmore G, Bozorgmehr N, Delyea C, Koleva P, Namdar A, Elahi S. Erythroid Suppressor Cells Compromise Neonatal Immune Response against *Bordetella pertussis*. JI. 2017 Sep 15;199(6):2081–95.

59. Hermiston ML, Xu Z, Weiss A. CD45: A Critical Regulator of Signaling Thresholds in Immune Cells. Annu Rev Immunol. 2003 Apr;21(1):107–37.

60. Trowbridge IS, Thomas ML. CD45: An Emerging Role as a Protein Tyrosine Phosphatase Required for Lymphocyte Activation and Development. Annu Rev Immunol. 1994 Apr;12(1):85–116.

61. Tchilian EZ, Beverley PCL. Altered CD45 expression and disease. Trends in Immunology. 2006 Mar;27(3):146–53.

62. Pingel JT, Thomas ML. Evidence that the leukocyte-common antigen is required for antigen-induced T lymphocyte proliferation. Cell. 1989 Sep 22;58(6):1055–65.

63. Grzywa TM, Nowis D, Golab J. The role of CD71+ erythroid cells in the regulation of the immune response. Pharmacology & Therapeutics. 2021 Dec;228:107927.

64. Wang L, Rubinstein R, Lines JL, Wasiuk A, Ahonen C, Guo Y, et al. VISTA, a novel mouse Ig superfamily ligand that negatively regulates T cell responses. Journal of Experimental Medicine. 2011 Mar 14;208(3):577–92.

65. Huang X, Zhang X, Li E, Zhang G, Wang X, Tang T, et al. VISTA: an immune regulatory protein checking tumor and immune cells in cancer immunotherapy. J Hematol Oncol. 2020 Dec;13(1):83.

66. Nowak EC, Lines JL, Varn FS, Deng J, Sarde A, Mabaera R, et al. Immunoregulatory functions of VISTA. Immunol Rev. 2017 Mar;276(1):66–79.

67. Yuan L, Tatineni J, Mahoney KM, Freeman GJ. VISTA: A Mediator of Quiescence and a Promising Target in Cancer Immunotherapy. Trends in Immunology. 2021 Mar;42(3):209–27.

68. Wang L, Le Mercier I, Putra J, Chen W, Liu J, Schenk AD, et al. Disruption of the immune-checkpoint *VISTA* gene imparts a proinflammatory phenotype with predisposition to the development of autoimmunity. Proc Natl Acad Sci USA. 2014 Oct 14;111(41):14846–51.

69. Shahbaz S, Bozorgmehr N, Koleva P, Namdar A, Jovel J, Fava RA, et al. CD71+VISTA+ erythroid cells promote the development and function of regulatory T cells through TGF-β. Marrack P, editor. PLoS Biol. 2018 Dec 14;16(12):e2006649.

70. Chen W, Jin W, Hardegen N, Lei K jian, Li L, Marinos N, et al. Conversion of Peripheral CD4+CD25− Naive T Cells to CD4+CD25+ Regulatory T Cells by TGF-β Induction of Transcription Factor Foxp3. Journal of Experimental Medicine. 2003 Dec 15;198(12):1875–86.

71. Peng Y, Laouar Y, Li MO, Green EA, Flavell RA. TGF-β regulates *in vivo* expansion of Foxp3-expressing CD4 $^{+}$ CD25 $^{+}$ regulatory T cells responsible for protection against diabetes. Proc Natl Acad Sci USA. 2004 Mar 30;101(13):4572–7.

72. Marie JC, Letterio JJ, Gavin M, Rudensky AY. TGF-β1 maintains suppressor function and Foxp3 expression in CD4+CD25+ regulatory T cells. Journal of Experimental Medicine. 2005 Apr 4;201(7):1061–7.

73. Sakaguchi S, Sakaguchi N, Shimizu J, Yamazaki S, Sakihama T, Itoh M, et al. Immunologic tolerance maintained by CD25 $^{+}$ CD4 $^{+}$ regulatory T cells: their common role in controlling autoimmunity, tumor immunity, and transplantation tolerance: Tolerance by CD25 $^{+}$ CD4 $^{+}$ T cells. Immunological Reviews. 2001 Aug;182(1):18–32.

74. Levéen P, Larsson J, Ehinger M, Cilio CM, Sundler M, Sjöstrand LJ, et al. Induced disruption of the transforming growth factor beta type II receptor gene in mice causes a lethal inflammatory disorder that is transplantable. Blood. 2002 Jul 15;100(2):560–8.

75. Gorelik L, Flavell RA. Abrogation of TGFβ Signaling in T Cells Leads to Spontaneous T Cell Differentiation and Autoimmune Disease. Immunity. 2000 Feb;12(2):171–81.

76. Lucas PJ, Kim SJ, Melby SJ, Gress RE. Disruption of T Cell Homeostasis in Mice Expressing a T Cell–Specific Dominant Negative Transforming Growth Factor β II Receptor. Journal of Experimental Medicine. 2000 Apr 3;191(7):1187–96.

77. Dröge W. Free Radicals in the Physiological Control of Cell Function. Physiological Reviews. 2002 Jan 1;82(1):47–95.

78. Srivastava MK, Sinha P, Clements VK, Rodriguez P, Ostrand-Rosenberg S. Myeloid-Derived Suppressor Cells Inhibit T-Cell Activation by Depleting Cystine and Cysteine. Cancer Res. 2010 Jan 1;70(1):68–77.

79. Sareila O, Kelkka T, Pizzolla A, Hultqvist M, Holmdahl R. NOX2 Complex–Derived ROS as Immune Regulators. Antioxidants & Redox Signaling. 2011 Oct 15;15(8):2197–208.

80. Kraaij MD, Savage NDL, van der Kooij SW, Koekkoek K, Wang J, van den Berg JM, et al. Induction of regulatory T cells by macrophages is dependent on production of reactive oxygen species. Proc Natl Acad Sci USA. 2010 Oct 12;107(41):17686–91.

81. El Kasmi KC, Qualls JE, Pesce JT, Smith AM, Thompson RW, Henao-Tamayo M, et al. Toll-like receptor–induced arginase 1 in macrophages thwarts effective immunity against intracellular pathogens. Nat Immunol. 2008 Dec;9(12):1399–406.

82. Pesce JT, Ramalingam TR, Mentink-Kane MM, Wilson MS, El Kasmi KC, Smith AM, et al. Arginase-1–Expressing Macrophages Suppress Th2 Cytokine–Driven Inflammation and Fibrosis. Kazura JW, editor. PLoS Pathog. 2009 Apr 10;5(4):e1000371.

83. Bolyen E, Rideout JR, Dillon MR, Bokulich NA, Abnet CC, Al-Ghalith GA, et al. Reproducible, interactive, scalable and extensible microbiome data science using QIIME 2. Nat Biotechnol. 2019 Aug;37(8):852–7.

84. Chen L, Wang J, Liu J, Wang H, Hillyer CD, Blanc L, et al. Dynamic changes in murine erythropoiesis from birth to adulthood: implications for the study of murine models of anemia. Blood Advances. 2021 Jan 12;5(1):16–25.

85. Schloss PD, Schubert AM, Zackular JP, Iverson KD, Young VB, Petrosino JF. Stabilization of the murine gut microbiome following weaning. Gut Microbes. 2012 Jul 14;3(4):383–93.

86. Bao Y, Dong C, Ji J, Gu Z. Dysregulation of gut microbiome is linked to disease activity of rheumatic diseases. Clin Rheumatol. 2020 Sep;39(9):2523–8.

87. Koh JH, Kim WU. Dysregulation of gut microbiota and chronic inflammatory disease: from epithelial defense to host immunity. Exp Mol Med. 2017 May;49(5):e337–e337.

88. Chen W, Wu J, Xie A. Cytokine regulation of immune tolerance. Burn Trauma. 2014;2(1):11.

89. Harrison OJ, Powrie FM. Regulatory T cells and immune tolerance in the intestine. Cold Spring Harb Perspect Biol. 2013 Jul 1;5(7):a018341.

90. Neely HR, Flajnik MF. Emergence and Evolution of Secondary Lymphoid Organs. Annu Rev Cell Dev Biol. 2016 Oct 6;32(1):693–711.

91. Kung C, Pingel JT, Heikinheimo M, Klemola T, Varkila K, Yoo LI, et al. Mutations in the tyrosine phosphatase CD45 gene in a child with severe combined immunodeficiency disease. Nat Med. 2000 Mar;6(3):343–5.

92. Byth KF, Conroy LA, Howlett S, Smith AJ, May J, Alexander DR, et al. CD45-null transgenic mice reveal a positive regulatory role for CD45 in early thymocyte development, in the selection of CD4+CD8+ thymocytes, and B cell maturation. Journal of Experimental Medicine. 1996 Apr 1;183(4):1707–18.

93. Tchilian EZ, Wallace DL, Wells RS, Flower DR, Morgan G, Beverley PCL. A Deletion in the Gene Encoding the CD45 Antigen in a Patient with SCID. J Immunol. 2001 Jan 15;166(2):1308–13.

94. Han LW, Shi Y, Paquette A, Wang L, Bammler TK, Mao Q. Key hepatic metabolic pathways are altered in germ-free mice during pregnancy. Lehmler HJ, editor. PLoS ONE. 2021 Mar 12;16(3):e0248351.

95. Faas MM, Liu Y, Borghuis T, van Loo-Bouwman CA, Harmsen H, de Vos P. Microbiota Induced Changes in the Immune Response in Pregnant Mice. Front Immunol. 2020 Jan 9;10:2976.

96. Khan I, Ullah N, Zha L, Bai Y, Khan A, Zhao T, et al. Alteration of Gut Microbiota in Inflammatory Bowel Disease (IBD): Cause or Consequence? IBD Treatment Targeting the Gut Microbiome. Pathogens. 2019 Aug 13;8(3):126.

97. Kaakoush NO, Day AS, Huinao KD, Leach ST, Lemberg DA, Dowd SE, et al. Microbial Dysbiosis in Pediatric Patients with Crohn's Disease. J Clin Microbiol. 2012 Oct;50(10):3258–66.

98. Singh VP, Proctor SD, Willing BP. Koch's postulates, microbial dysbiosis and inflammatory bowel disease. Clinical Microbiology and Infection. 2016 Jul;22(7):594–9.

99. Hanson LÅ, Korotkova M, Lundin S, Håversen L, Silfverdal SA, Mattsby-Baltzer I, et al. The Transfer of Immunity from Mother to Child. Annals of the New York Academy of Sciences. 2003 Apr;987(1):199–206.

100. Hung LY, Parathan P, Boonma P, Wu Q, Wang Y, Haag A, et al. Antibiotic exposure postweaning disrupts the neurochemistry and function of enteric neurons mediating colonic motor activity. American Journal of Physiology-Gastrointestinal and Liver Physiology. 2020 Jun 1;318(6):G1042–53.

101. Kostic AD, Howitt MR, Garrett WS. Exploring host–microbiota interactions in animal models and humans. Genes Dev. 2013 Apr 1;27(7):701–18.

102. Mueller S, Saunier K, Hanisch C, Norin E, Alm L, Midtvedt T, et al. Differences in Fecal Microbiota in Different European Study Populations in Relation to Age, Gender, and Country: a Cross-Sectional Study. Appl Environ Microbiol. 2006 Feb;72(2):1027–33.

103. Finnicum CT, Beck JJ, Dolan CV, Davis C, Willemsen G, Ehli EA, et al. Cohabitation is associated with a greater resemblance in gut microbiota which can impact cardiometabolic and inflammatory risk. BMC Microbiol. 2019 Dec;19(1):230.

104. Song SJ, Lauber C, Costello EK, Lozupone CA, Humphrey G, Berg-Lyons D, et al. Cohabiting family members share microbiota with one another and with their dogs. eLife. 2013 Apr 16;2:e00458.

105. Dill-McFarland KA, Tang ZZ, Kemis JH, Kerby RL, Chen G, Palloni A, et al. Close social relationships correlate with human gut microbiota composition. Sci Rep. 2019 Dec;9(1):703.

106. Malmuthuge N, Griebel PJ, Guan LL. The Gut Microbiome and Its Potential Role in the Development and Function of Newborn Calf Gastrointestinal Tract. Front Vet Sci [Internet]. 2015 Sep 23 [cited 2022 Aug 22];2. Available from: http://journal.frontiersin.org/Article/10.3389/fvets.2015.00036/abstract

107. Van den Abbeele P, Van de Wiele T, Verstraete W, Possemiers S. The host selects mucosal and luminal associations of coevolved gut microorganisms: a novel concept. FEMS Microbiol Rev. 2011 Jul;35(4):681–704.

108. Arrieta MC, Stiemsma LT, Dimitriu PA, Thorson L, Russell S, Yurist-Doutsch S, et al. Early infancy microbial and metabolic alterations affect risk of childhood asthma. Sci Transl Med [Internet]. 2015 Sep 30 [cited 2022 Aug 22];7(307). Available from: https://www.science.org/doi/10.1126/scitranslmed.aab2271

109. Torres J, Hu J, Seki A, Eisele C, Nair N, Huang R, et al. Infants born to mothers with IBD present with altered gut microbiome that transfers abnormalities of the adaptive immune system to germ-free mice. Gut. 2020 Jan;69(1):42–51.